USAFA-TR-76-9

THE EFFECT OF THRUST VECTORING ON AIRCRAFT MANEUVERING

LT COL DUANE M. DAVIS
MAJOR JERRY D. HINES

DEPARTMENT OF AERONAUTICS
USAF ACADEMY, COLORADO 80840

JUNE 1976
FINAL REPORT

APPROVED FOR PUBLIC RELEASE; DISTRIBUTION UNLIMITED

DEAN OF THE FACULTY
UNITED STATES AIR FORCE ACADEMY
COLORADO 80840

DISCLAIMER NOTICE

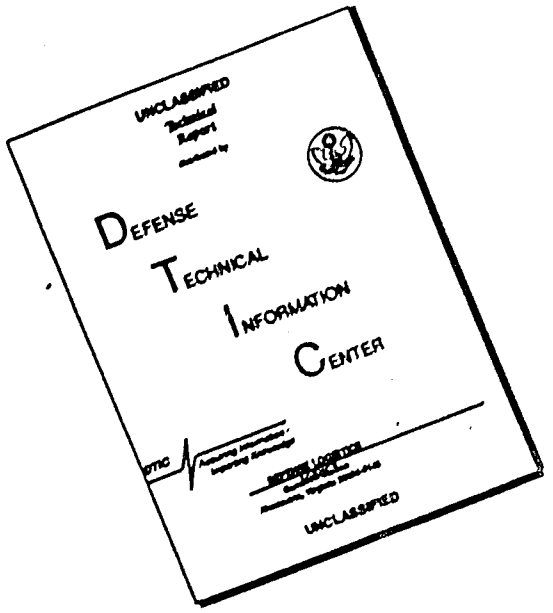

THIS DOCUMENT IS BEST QUALITY AVAILABLE. THE COPY FURNISHED TO DTIC CONTAINED A SIGNIFICANT NUMBER OF PAGES WHICH DO NOT REPRODUCE LEGIBLY.

Editorial Review by Major R.B. Donovan
Department of English and Fine Arts
USAF Academy, Colorado 80840

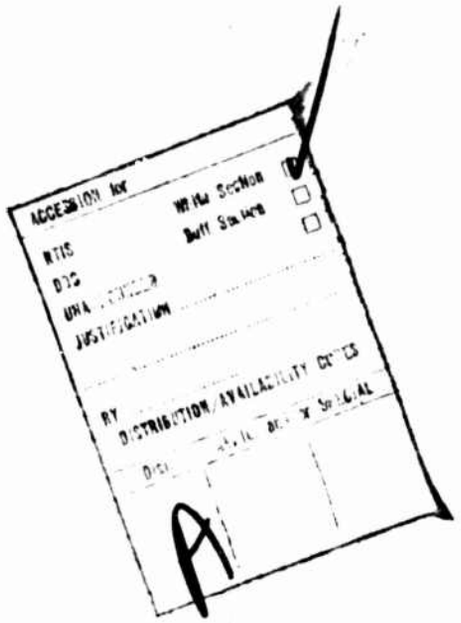

This research report is presented as a competent treatment of the subject, worthy of publication. The United States Air Force Academy vouches for the quality of the research, without necessarily endorsing the opinions and conclusions of the author.

This report has been cleared for open publication and/or public release by the appropriate Office of Information in accordance with AFR 190-17 and DODD 5230.9. There is no objection to unlimited distribution of this report to the public at large, or by DDC to the National Technical Information Service.

This research report has been reviewed and is approved for publication.

PHILIP J. ERDLE, Colonel, USAF
Vice Dean of the Faculty

Additional copies of this document are available through the National Technical Information Service, U.S. Department of Commerce, 5285 Port Royal Road, Springfield, VA 22151.

UNCLASSIFIED

REPORT DOCUMENTATION PAGE

READ INSTRUCTIONS BEFORE COMPLETING FORM

(14) USAFA-TR-76-9

(6) The Effect of Thrust Vectoring on Aircraft Maneuvering.

(9) Final Report. Oct 1971 - Aug 1973

(10) Lt Col Duane M. Davis
Major Jerry D. Hines

Department of Aeronautics (DFAN)
USAF Academy, CO 80840

(11) Air Force Aero Propulsion Laboratory
Wright-Patterson AFB, OH 45433

June 1976

56

Dean of the Faculty
USAF Academy, CO 80840

(12) 54p.

Unclassified

Approved for public release; distribution unlimited

thrust vector control
air to air combat
optimization
maneuverability

A 3-dimensional minimum time turn optimal control problem was used as a framework for a preliminary investigation of the effects of thrust vectoring. Two basic configurations were used for aircraft in the study. They were the same except that one has the thrust vector fixed along the longitudinal axis, and the thrust vector for the other is free to move in the aircraft vertical plane. The effect of initial velocity, weight penalty and thrust-to-weight ratio were investigated. The results show a definite advantage for the thrust vectored aircraft for most of the conditions investigated and the possibility of an advantage for the others.

AB

20. Therefore, more detailed analysis of the effect of thrust vectoring on combat maneuverability is justified.

PREFACE

The work reported here was performed for the Air Force Aero Propulsion Laboratory, Wright-Patterson AFB, Ohio, and was accomplished by Lt Col Duane M. Davis and Major Jerry D. Hines primarily at the United States Air Force Academy, Colorado, between October 1971 and August 1973.

TABLE OF CONTENTS

LIST OF FIGURES

LIST OF TABLES

INTRODUCTION

The purpose of this investigation was to determine whether more complex and detailed studies of the effects of thrust vectoring on air-to-air combat maneuverability were advisable. The minimum time turn was selected as the maneuver to study in order to keep the cost of the study down. Turning capability is very important in air-to-air combat, and since for given initial conditions, minimum radius is also obtained in a minimum time turn, it was possible to study two important aspects of the problem without a great deal of complexity.

A mathematical representation of an aircraft similar to the F-4E was created. This model was used in a first-order gradient optimization procedure. The output of the computer program was a trajectory for a minimum time turn for the selected initial conditions. In general, for each set of initial conditions two trajectories were produced, one for an aircraft without thrust vectoring capability and one for an aircraft with thrust vectoring capability. All cases were for 180° of turn. For most cases, the angle of turn and the flight path angle at the final time were the only constraints. However, in some cases (high speed weight penalty and high speed thrust ratio) it was necessary to also constrain the final altitude. These constraints were employed in an attempt to produce results which could be used to judge whether the vectored or nonvectored thrust configuration had a combat advantage at the end of the 180° turn.

The effects of initial velocity, thrust-to-weight ratio and weight penalty were investigated. Even using the most simplified model of the air combat situation that could be expected to provide a reasonable basis for comparison, the computer time required was high. Satisfactory convergence was difficult to obtain in the cases where the effect of thrust-to-weight ratio was investigated. In the weight penalty investigation, weight was added to the thrust-vectored configuration until the weight was 125% of the conventional aircraft. In general, varying the thrust to weight ratio may be accomplished by changing either the weight or the thrust. The purpose of the weight penalty study was to determine the amount of weight penalty, associated with mechanizing the thrust vectoring, that would nullify the advantage of thrust vectoring. Therefore, several thrust-vectored cases with increased weights were compared with the basic conventional aircraft case. The purpose of the thrust to weight ratio investigation was to identify the range of thrust to weight ratios where thrust vectoring provided the biggest payoff. Therefore, this study was conducted by investigating pairs of aircraft (one conventional and one thrust-vectored) at the same thrust to weight ratio.

We recognize the minimum time turn criteria for the optimization formulation is not the best criteria to compare combat capability. However, it was chosen so that an initial investigation could

be conducted at an acceptable cost. The study shows that the thrust-vectored aircraft has a capability to maneuver in areas where the conventional aircraft does not. The trajectories of the thrust-vectored aircraft represent the bounds of this capability. In the combat situation, the thrust-vectored aircraft would not be flown along a minimum time turn trajectory in most cases. The difference between the conventional and thrust-vectored trajectories represents the additional capability for combat maneuver that gives the thrust-vectored aircraft an advantage in combat maneuver. The way that this capability is employed is up to the individual pilot and depends upon the situation. In combat it is generally desirable to maintain as high an energy level as possible and the employment of thrust vectoring lowers the energy level of the aircraft. However, the objective of air combat is to shoot down the other aircraft and if a sacrifice of energy level is necessary to achieve this objective, it is the correct thing to do. The reader should keep these points in mind as he evaluates the results of this study.

THEORY

The program which computes the optimal trajectories uses a general first-order gradient algorithm for optimal control problems with known initial conditions and unknown final time. The state equations and adjoint equations are integrated using a third-order modified Euler integration scheme [7]. All partial derivatives needed by the program are computed using finite difference relations. Some double-precision computation is necessary to obtain accurate third-order partial derivatives. The state equations are the point mass equations of motion for the aircraft. Internally, the program uses a non-dimensional form of the equations. The program contains formulation for two types of aircraft. One is the conventional aircraft with the thrust vector fixed along the longitudinal axis. The other is a thrust-vectored aircraft where the thrust can be directed throughout the aircraft's vertical plane.

The basic problem can be stated as follows:

For a dynamic system governed by first-order differential equations of the form

$$\dot{x} = f(x,u,t), \qquad (1)$$

determine the control history u(t) and the final time which optimizes a performance index of the form

$$I = \beta\,(x_f, t_f) + \int_{t_o}^{t_f} F(x,u,t)dt\,. \tag{2}$$

In these equations, x is an n-component state vector, u is an m-component control vector, and t is the independent variable time. The initial conditions at t_o

$$x(t_o) = x_o \tag{3}$$

are known. One or more terminal constraints are imposed on the solution. The terminal constraints will be denoted by the ν-component vector

$$\psi(x_f, t_f) = 0 \tag{4}$$

where each component is a functional relationship which must be satisfied at t_f.

The necessary condition for an optimal solution is that the total variation in the performance index, I, due to variations, $\delta u(t)$, is zero; i.e.,

$$dI = 0\,, \tag{5}$$

where the constraints in equations (1), (3) and (4) are satisfied. Equations (1) and (4) can be adjoined to equation (2) with the adjoint variables $\lambda(t)$ and Lagrange multipliers ν to give

$$I = \beta + \nu^T \psi + \int_{t_o}^{t_f} \{F(x,u,t) + \lambda^T(t)\,[f(x,u,t)-\dot{x}]\}dt\,. \tag{6}$$

Differentiation followed by integration by parts gives

$$dI = \left(\frac{\partial \beta}{\partial t} + \nu^T \frac{\partial \Psi}{\partial t} + F + \lambda^T \dot{x}\right) dt_f$$

$$+ \left(\frac{\partial \beta}{\partial x} + \nu^T \frac{\partial \Psi}{\partial x} - \lambda^T\right) dx_f + \lambda_o{}^T \delta x_o$$

$$+ \int_{t_o}^{t_f} \left[\left(-\frac{\partial H}{\partial x} + \dot{\lambda}^T\right) \delta x + \frac{\partial H}{\partial u} \delta u\right] dt , \qquad (7)$$

where the Hamiltonian H is defined by

$$H \quad F(x,u,t) + \lambda^T(t)\ f(x,u,t) \qquad (8)$$

and

$$\delta x = dx - \dot{x}dt . \qquad (9)$$

The adjoint variables can be chosen to satisfy the conditions

$$\dot{\lambda}^T = -\frac{\partial H}{\partial x} = -\lambda^T \frac{\partial f}{\partial x} - \frac{\partial F}{\partial x} \qquad (10)$$

and

$$\lambda_f^T - \frac{\partial \beta}{\partial x} + \nu^T \frac{\partial \Psi}{\partial x} . \qquad (11)$$

By imposing the additional condition on ν that

$$\Omega(\nu) = \frac{\partial \beta}{\partial t} + \nu^T \frac{\partial \Psi}{\partial t} + F + \lambda^T \dot{x} = 0 , \qquad (12)$$

the variation in the performance index reduces to

$$dI = \int_{t_o}^{t_f} \frac{\partial H}{\partial u} \delta u\ dt . \qquad (13)$$

Since the variations in u(t) are arbitrary, a stationary value of I can exist only when

$$\frac{\partial H}{\partial u} = 0 ; \quad t_o < t < t_f . \qquad (14)$$

In effect, the optimization problem has been transformed into a two-point boundary value problem with 2n differential equations and mixed initial and terminal constraints where u(t) satisfies equation (14). The 2n differential equations are given in equations (1) and (10), and the initial and terminal constraints are given by equations (3) and (11).

The vector ν is so far unspecified and must be found from the variation of the terminal constraints. In general, $\lambda(t)$ can be expressed as a linear function of ν as

$$\lambda(t) = p(t) + R(t)\nu, \tag{15}$$

where the n-component vector $p(t)$ and the $n \times \ell$ matrix $R(t)$ are called influence functions and are defined by the differential equations

$$\dot{p} = -\left(\frac{\partial f}{\partial x}\right)^T p - \left(\frac{\partial F}{\partial x}\right)^T \tag{16}$$

and

$$\dot{R} = -\left(\frac{\partial f}{\partial x}\right)^T R, \tag{17}$$

where

$$p_{t_f}^T = \frac{\partial \beta}{\partial x} \tag{18}$$

and

$$R_{t_f}^T = \frac{\partial \Psi}{\partial x}. \tag{19}$$

In terms of the influence functions, the first-order variations in the terminal constraints are

$$d\Psi = \dot{\Psi} dt_f + \int_{t_o}^{t_f} R^T \frac{\partial f}{\partial u} \delta u \, dt, \tag{20}$$

where

$$\dot{\Psi} = \frac{\partial \Psi}{\partial t} + \frac{\partial \Psi}{\partial x} f. \tag{21}$$

Equations (12) and (20) supply the information to determine the vector ν and the final time t_f.

The computational algorithm is as follows:

Step (a). Using an initial estimate of the control history u(t), integrate the equations

$$\dot{x} = f(x,u,t) \tag{1}$$

forward to an estimated final time t_f. The terminal constraints (4) will not be satisfied.

Step (b). Compute the influence functions at each integration point along the trajectory by integrating the equations

$$\dot{p}(t) = -\left(\frac{\partial f}{\partial x}\right)^T p - \left(\frac{\partial F}{\partial x}\right)^T \tag{16}$$

and

$$\dot{R}(t) = -\left(\frac{\partial f}{\partial x}\right)^T R \tag{17}$$

backward using the terminal conditions

$$p^T_{t_f} = \frac{\partial \beta}{\partial x} \tag{18}$$

and

$$R^T_{t_f} = \frac{\partial \Psi}{\partial x} . \tag{19}$$

Step (c). Using an estimate of ν, compute

$$\lambda(t) = p(t) + R(t)\,\nu, \tag{15}$$

$$\frac{\partial H}{\partial u} = \frac{\partial F}{\partial u} + \lambda^T \frac{\partial f}{\partial u} , \tag{22}$$

$$\frac{\partial^2 H}{\partial u^2} = \frac{\partial^2 F}{\partial u^2} + \lambda^T \frac{\partial^2 f}{\partial u^2} , \tag{23}$$

and

$$\frac{\partial^2 H}{\partial u^2} = \frac{\partial^2 F}{\partial u^2} + \lambda^T \frac{\partial^2 f}{\partial u^2} \tag{24}$$

at each integration point along the trajectory. Simultaneously, compute corrections δu from the relation

$$\frac{\partial H}{\partial u} + \frac{\partial^2 H}{\partial u^2} \delta u + \frac{1}{2} \delta u^T \frac{\partial^3 H}{\partial u^3} \delta u = 0. \tag{25}$$

Step (d). With these values of $\delta u(t)$ and an estimated correction to the final time, dt_f, compute the predicted variation in the terminal constraints from the relation

$$d\Psi(\nu, dt_f) = \dot{\Psi}\, dt_f + \int_{t_o}^{t_f} R^T \frac{\partial f}{\partial u} \delta u \, dt. \tag{20}$$

Also, evaluate the transversality function

$$\Omega(\nu) = \frac{\partial \beta}{\partial t} + \nu^T \frac{\partial \Psi}{\partial t} + H. \tag{12}$$

Step (e). Vary the values of ν and numerically compute the partial derivatives $\frac{\partial d\Psi}{\partial \nu}$ and $\frac{\partial^2 d\Psi}{\partial \nu^2}$. With these partial derivatives, improve the estimate of ν and dt_f using the relation

$$\begin{pmatrix} \nu' \\ dt_f' \end{pmatrix} = \begin{pmatrix} \nu \\ dt_f \end{pmatrix} - \left\{ \begin{pmatrix} \frac{\partial d\Psi}{\partial \nu} & \dot{\Psi} \\ \dot{\Psi} & 0 \end{pmatrix} - \frac{1}{2} \left[\begin{pmatrix} \frac{\partial d\Psi}{\partial \nu} & \dot{\Psi} \\ \dot{\Psi} & 0 \end{pmatrix}^{-1} \begin{pmatrix} \Psi + d\Psi \\ \Omega \end{pmatrix} \right]^T \right.$$

$$\left. \begin{pmatrix} \frac{\partial^2 d\Psi}{\partial \nu^2} & 0 \\ 0 & 0 \end{pmatrix} \right\}^{-1} \begin{pmatrix} \Psi + d\Psi \\ \Omega \end{pmatrix}. \tag{26}$$

Step (f). Iterate steps (c), (d), and (e) until

$$d\Psi(\nu, dt_f) = -\Psi(x_f, t_f) \quad (27)$$

and

$$\Omega(\nu) = 0 \quad (28)$$

are satisfied.

Step (g). When equations (27) and (28) have been satisfied, correct the estimates of $u(t)$ and t_f with

$$u'(t) = u(t) + \epsilon\, \delta u(t) \quad (29)$$

and

$$t'_f = t_f + \epsilon\, dt_f , \quad (30)$$

where ϵ is introduced to account for the nonlinearity of the problem. Using the improved estimate of $u(t)$ and t_f, repeat the process starting with step (a) until some test for convergence is met. Some combination of the degree to which equations (4) and (14) are satisfied is usually used.

AIRCRAFT EQUATIONS OF MOTION

Assuming zero sideslip angle and no side forces, the point mass equations of motion for the aircraft are

$$\frac{dx}{dt} = V \cos\gamma \cos\psi , \quad (31)$$

$$\frac{dy}{dt} = V \cos\gamma \sin\psi , \quad (32)$$

$$\frac{dz}{dt} = -V \sin\gamma , \quad (33)$$

$$m \frac{dV}{dt} = F_g \cos\alpha_T - D - W \sin\gamma - D_{ram} , \quad (34)$$

$$mV \frac{d\gamma}{dt} = L \cos\phi + F_g \sin\alpha_T \cos\phi - W \cos\gamma , \quad (35)$$

$$mV \cos\gamma \frac{d\psi}{dt} = L \sin\phi + F_g \sin\alpha_T \sin\phi , \quad (36)$$

$$L = C_L \rho V^2 S, \tag{37}$$

$$D = (C_{D_o} + KC_L^2) \rho V^2 S, \tag{38}$$

where

γ - flight path angle (positive up from the horizon),
ψ - heading angle,
σ - bank angle,
α_T - angle of thrust vector measured from the velocity vector (positive up).

The original direction of the velocity vector is the positive X direction, and the heading angle is measured from the positive X axis. The positive direction for the z axis is down. See Figures 1 and 2.

ATMOSPHERIC MODEL

Assuming that temperature varies linearly with altitude according to the relation

$$T = T_{SL} - \frac{T_{SL}\, h}{144000}, \tag{39}$$

where

T - temperature,
T_{SL} - sea level temperature,
h - altitude,

and that air is a perfect gas, an expression for the pressure ratio can be found of the form

$$\frac{p}{p_{SL}} = \left(\frac{T}{T_{SL}}\right)^{\frac{144000g}{RT_{SL}}}, \tag{40}$$

where

p - pressure,
p_{SL} - sea level pressure,
R - the gas constant for air.

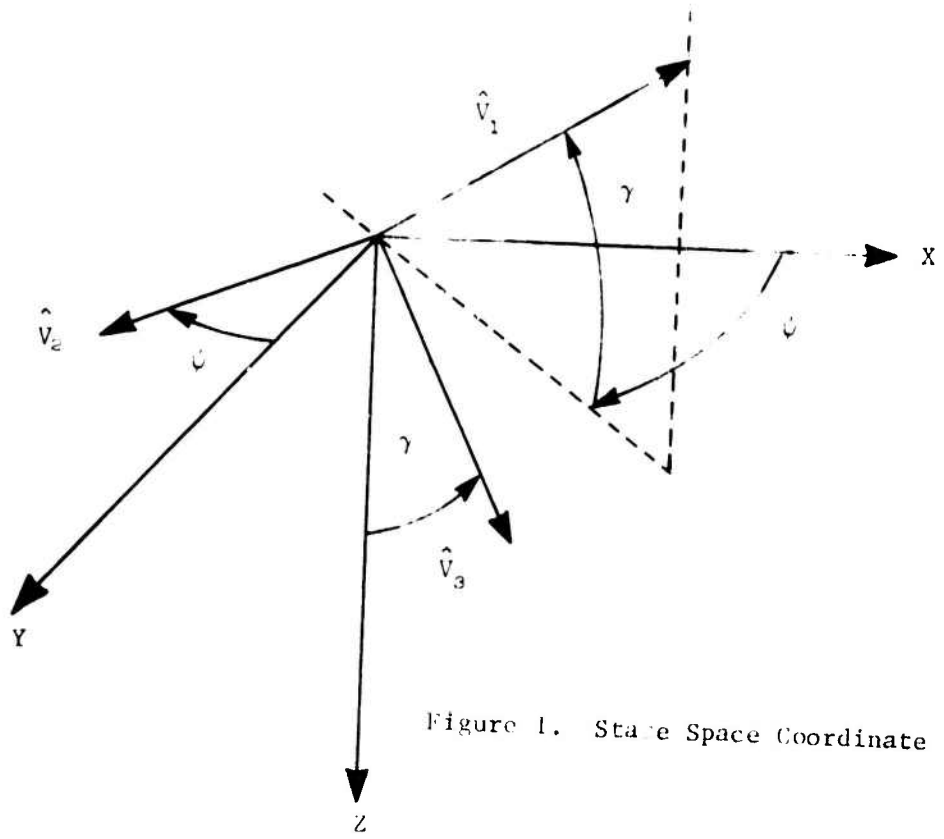

Figure 1. State Space Coordinate System

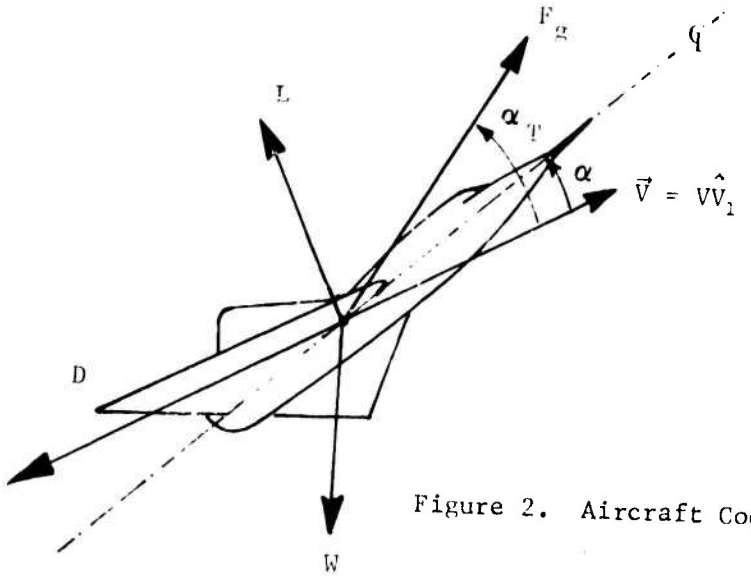

Figure 2. Aircraft Coordinate System

In terms of the non-dimensional altitude $z = -h/R_{min}$, the pressure and temperature ratios can be written as

$$\frac{T}{T_{SL}} = 1 - \frac{R_{min}}{144000} z , \tag{41}$$

where

R_{min} - minimum radius for a level turn at sea level

and

$$\frac{p}{p_{SL}} = \left(\frac{T}{T_{SL}}\right)^{5.2094} . \tag{42}$$

The density ratio is given by

$$\sigma \quad \frac{\rho}{\rho_{SL}} = \frac{(p/p_{SL})}{(T/T_{SL})} . \tag{43}$$

COMPUTATION OF GROSS THRUST

In general, the gross thrust is a function of Mach number, M, and altitude, h. At a given altitude, F_g may be approximated by

$$F_g = F_{go} + \frac{\partial F_g}{\partial M} (M-M_o) + \frac{1}{2} \frac{\partial^2 F_g}{\partial M^2} (M-M_o)^2 , \tag{44}$$

where F_{go} and the partials are functions of altitude evaluated at M_o. In turn, the F_{go}, $\frac{\partial F_g}{\partial M}$, and $\frac{\partial^2 F_g}{\partial M^2}$ can be approximated as functions of altitude using

$$F_{go} = C_{11} + C_{12} (h-h_o) + \frac{1}{2} C_{13} (h-h_o)^2 , \tag{45}$$

$$\frac{\partial F_{go}}{\partial M} = C_{21} + C_{22} (h-h_o) + \frac{1}{2} C_{23} (h-h_o)^2 , \tag{46}$$

and

$$\frac{\partial^2 F_{go}}{\partial M^2} = C_{31} + C_{32} (h-h_o) + \frac{1}{2} C_{33} (h-h_o)^2 . \tag{47}$$

Coefficients and engine data for the J79GE-17 engine with afterburner are given in DFAN TR 73-4.

COMPUTATION OF RAM DRAG

The ram drag is also a function of altitude and Mach number or velocity. The ram drag can be approximated by the relation

$$D_{ram} = \left(C_{D_{R_1}} \frac{1}{V} + C_{D_{R_2}}\right) \tfrac{1}{2} \rho V^2 S. \qquad (48)$$

$C_{D_{R_1}}$, $C_{D_{R_2}}$, and ram drag data for the J79GE-17 engine with afterburner are given in DFAN TR 73-4, along with a complete description of the computer program.

RESULTS AND DISCUSSION

Conditions. The effects of three parameters (initial velocity, weight penalty, thrust-to-weight ratio) were investigated. The initial conditions and terminal constraints which were not the same for all runs are given in Table I. Final conditions are given in Table II. All trajectories start at 20,000 ft, have a heading change of 180°, and end with the flight path angle equal to zero. Except where noted for the weight penalty investigation, the aircraft weight is 40,000 lbf, and for all cases it is constant throughout the turn. The wing area is 530 ft^2, and the maximum load factor is 7.33 at all altitudes and air speeds. With the exception of the column in Table I labeled T/W at SL, all thrust-to-weight ratios are for the initial conditions of the run. It should be noted that the thrust varies with altitude and, therefore, the thrust to weight ratio varies along the trajectory.

All runs were at maximum afterburner to maintain maximum energy for combat, although for the high speed conventional runs idle thrust would produce a tighter, faster turn. For all runs except 21 through 26, 38, 40, and 42, the final altitude was determined by the optimization process. For the runs mentioned the final altitude was constrained to be the same as that for the conventional aircraft run that the results were to be compared with. This was necessary because the final altitude which resulted otherwise was so far below the final altitude for the conventional run that no conclusion about combat advantage could be made. The nature of the optimization algorithm is such that the final altitude does not have to be exactly equal to the constraint, but in every case it is close to the constraint.

RUN	CONVENTIONAL OR THRUST-VECTORED	INITIAL VELOCITY ft/sec	T/W at SL	T/W at 20,000 ft	CONSTRAINED FINAL ALTITUDE ft	WEIGHT PENALTY lbf
1	C	400	1.039	0.480		
2	TV	400	1.039	0.480		
3	C	600	1.069	0.585		
4	TV	600	1.069	0.585		
5	C	800	1.206	0.722		
6	TV	800	1.206	0.722		
7	C	1000	1.450	0.891		
8	TV	1000	1.450	0.891		
9	C	1200	1.801	1.092		
10	TV	1200	1.801	1.092		
11	C	1400	2.259	1.326		
12	TV	1400	2.259	1.326		
13	C	600	1.069	0.585		
14	TV	↓	1.069	0.585		
15	TV	↓	1.018	0.557		2000
16	TV	↓	0.972	0.532		4000
17	TV	↓	0.930	0.508		6000
18	TV	↓	0.891	0.487		8000
19	TV	600	0.855	0.468		10000
20	C	1200	1.801	1.092		
21	TV	↓	1.801	1.092	24519	
22	TV	↓	1.715	1.040	↓	2000
23	TV	↓	1.637	0.990	↓	4000
24	TV	↓	1.566	0.950	↓	6000
25	TV	↓	1.501	0.910	↓	8000
26	TV	1200	1.441	0.870	24519	10000
27	C	600	1.069	0.585		
28	TV	↓	1.069	0.585		
29	C	↓	1.371	0.750		
30	TV	↓	1.371	0.750		
31	C	↓	1.828	1.000		
32	TV	↓	1.828	1.000		
33	C	↓	2.285	1.250		
34	TV	↓	2.285	1.250		
35	C	↓	2.742	1.500		
36	TV	600	2.742	1.500		
37	C	1200	1.801	1.092		
38	TV	↓	1.801	1.092	24519	
39	C	↓	2.061	1.250		
40	TV	↓	2.061	1.250	25637	
41	C	↓	2.473	1.500		
42	TV	1200	2.473	1.500	26807	

TABLE I. Initial Conditions and Terminal Constraints

RUN	CONVENTIONAL OR THRUST-VECTORED	TIME FOR TURN (sec)	FINAL VALUES			
			VELOCITY	X	Y	ALTITUDE
1	C	15.58	652	-1049	1088	14534
2	TV	15.32	599	- 950	1047	14714
3	C	13.32	714	- 529	1266	14394
4	TV	13.13	662	- 412	1221	14547
5	C	11.43	786	- 227	1486	14353
6	TV	11.27	738	- 108	1332	14450
7	C	11.91	820	530	6611	18077
8	TV	10.50	750	160	1724	14605
9	C	14.06	888	2299	8444	24519
10	TV	11.50	773	1298	5323	15818
11	C	15.13	824	3716	10476	23252
12	TV	12.65	792	2663	7929	18187
13	C	13.32	714	- 529	1266	14394
14	TV	13.13	662	- 412	1221	14547
15	TV	13.61	670	- 456	1080	14266
16	TV	14.10	681	- 501	1050	14003
17	TV	14.56	685	- 538	964	13747
18	TV	15.02	693	- 560	916	13479
19	TV	15.47	699	- 594	898	13223
20	C	14.06	888	2299	8444	24519
21	TV	13.16	699	1793	6310	24526
22	TV	13.48	701	1764	6601	24552
23	TV	13.88	703	1678	6918	24539
24	TV	14.25	704	1625	7208	24560
25	TV	14.75	704	1478	7533	24524
26	TV	15.16	700	1402	7801	24540
27	C	13.32	714	- 529	1266	14394
28	TV	13.13	662	- 412	1221	14547
29	C	12.76	752	- 489	1162	14454
30	TV	12.54	685	- 360	1122	14648
31	C	12.03	806	- 443	1125	14552
32	TV	11.78	715	- 298	1107	14818
33	C	11.76	890	- 714	1230	14563
34	TV	11.13	741	- 254	1057	14967
35	C	11.74	1008	-1225	1254	14411
36	TV	10.57	760	- 222	1012	15120
37	C	14.06	888	2299	8444	24519
38	TV	13.16	699	1793	6310	24526
39	C	14.22	897	2318	7940	25637
40	TV	13.22	681	1831	5276	25637
41	C	14.27	951	2435	7609	26807
42	TV	13.15	687	1882	3734	26804

TABLE II. Terminal Conditions

Runs 1 through 12 represent the investigation of the effects of initial velocity. Runs 13 through 26 are for the effect of weight penalty, and runs 27 through 42 are for the effect of thrust-to-weight ratio. Runs 13 and 27 are the same as run number 3. Runs 20 and 37 are the same as run number 9. Runs 14 and 28 are the same as run number 4. The data was repeated so that all of the data on a particular aspect of the investigation would be presented together and to make it easier to discuss the results. All velocities are given in ft/sec, distances in feet, and time in seconds.

Initial Velocity. The greatest differences between the conventional and thrust-vectored aircraft were found for initial velocities above the corner velocity, which for the initial altitude of 20,000 ft was about 900 ft/sec. The corner velocity is the stall speed at maximum load factor and for a level constant speed turn, it is the velocity for a minimum time, minimum radius turn. For all runs with an initial velocity below the corner velocity, the thrust-vectored aircraft ended up about 50 ft/sec slower, inside, above, and slightly in front of the conventional aircraft with slant ranges less than 190 ft (Table III). The slant range referred to in Table III is the line of sight distance between the two aircraft. The thrust-vectored aircraft has the combat advantage, but the advantage is small. At first it might seem that the conventional aircraft has the advantage because it is behind the thrust-vectored aircraft. However, it is not possible for the conventional aircraft to bring guns to bear on the thrust-vectored aircraft since it is turning at its maximum rate and is outside of, below, and faster than the thrust-vectored aircraft and it is one to two degrees short of completing its turn. On the other hand, the thrust-vectored aircraft may climb and slow down slightly to end up behind the conventional aircraft and use its thrust vector capability to bring guns to bear. One of the outcomes of tests on the Harrier aircraft such as those reported in References 1 and 2 was the demonstration of the unique pointing capability that thrust vectoring provides.

For speeds above the corner velocity it is more difficult to determine which aircraft has the advantage. Paths over the ground for runs 1 through 12 are plotted in Figure 3. Altitude is plotted in Figure 4 for runs 3, 4, 9, and 10 against time divided by final time (T/TF). In Figure 5, velocity is plotted against non-dimensional time for runs 3, 4, 9, and 10. With this information, the reader may visualize the trajectories and sequence of events in three dimensions. Consider runs 7 and 8 (initial velocity 1000 ft/sec) where the thrust-vectored aircraft is 4680 feet inside, 3550 feet below, and 99 ft/sec slower than the conventional aircraft. Holding the final altitude of the thrust-vectored aircraft closer to that of the conventional aircraft will result in bringing the paths of the two aircraft over the ground closer together as well as in slowing down the thrust-vectored aircraft. This should allow the thrust-vectored aircraft to obtain a position where its guns can be brought to bear on the conventional aircraft.

RUN	INITIAL VELOCITY	C OR TV	TIME	POSITION AT TIME GIVEN					SLANT RANGE
				ψ	x	y	ALTITUDE	VELOCITY	
1	400	C	15.32	178	- 895	1083	14538	655	
2	400	TV	15.32	180	- 950	1047	14714	599	188
3	600	C	13.13	179	- 402	1264	14398	717	
4	600	TV	13.13	180	- 412	1221	14547	662	157
5	800	C	12.27	178	- 47	1481	14357	791	
6	800	TV	12.27	180	- 108	1332	14450	738	186
7	1000	C	10.50	160	1695	6404	18155	849	
8	1000	TV	10.50	180	160	1724	14605	750	6071
9	1200	C	11.50	144.5	4459	7758	24200	960	
10	1200	TV	11.50	180	1298	5323	15818	773	9283
11	1400	C	12.65	146	5730	9710	23110	945	
12	1400	TV	12.65	180	2663	7929	18187	792	6067

TABLE III. Position at the End of 180° Turn for Thrust-Vectored Aircraft
Effect of Initial Velocity

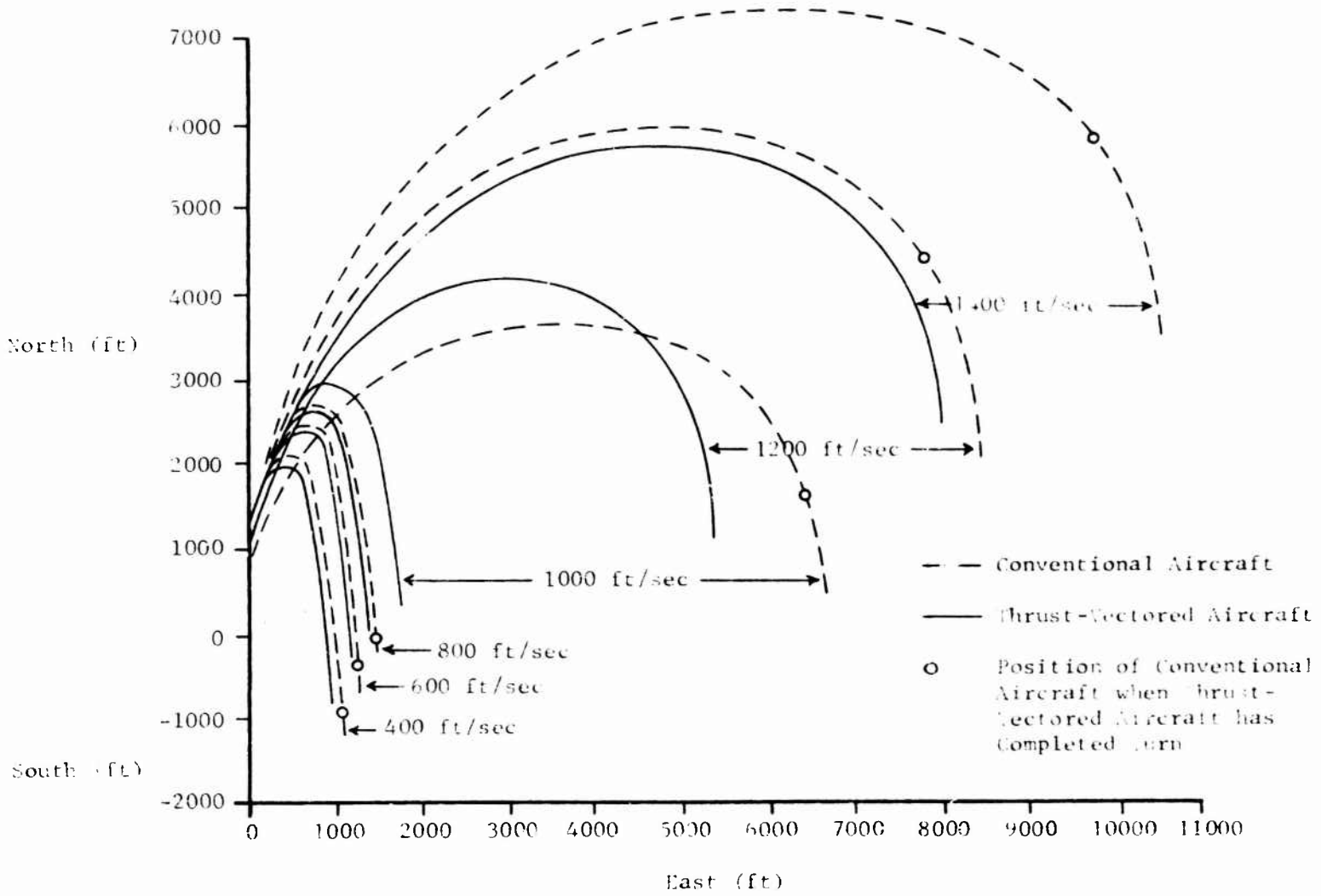

Figure 3. Ground Trace-Effect of Initial Velocity

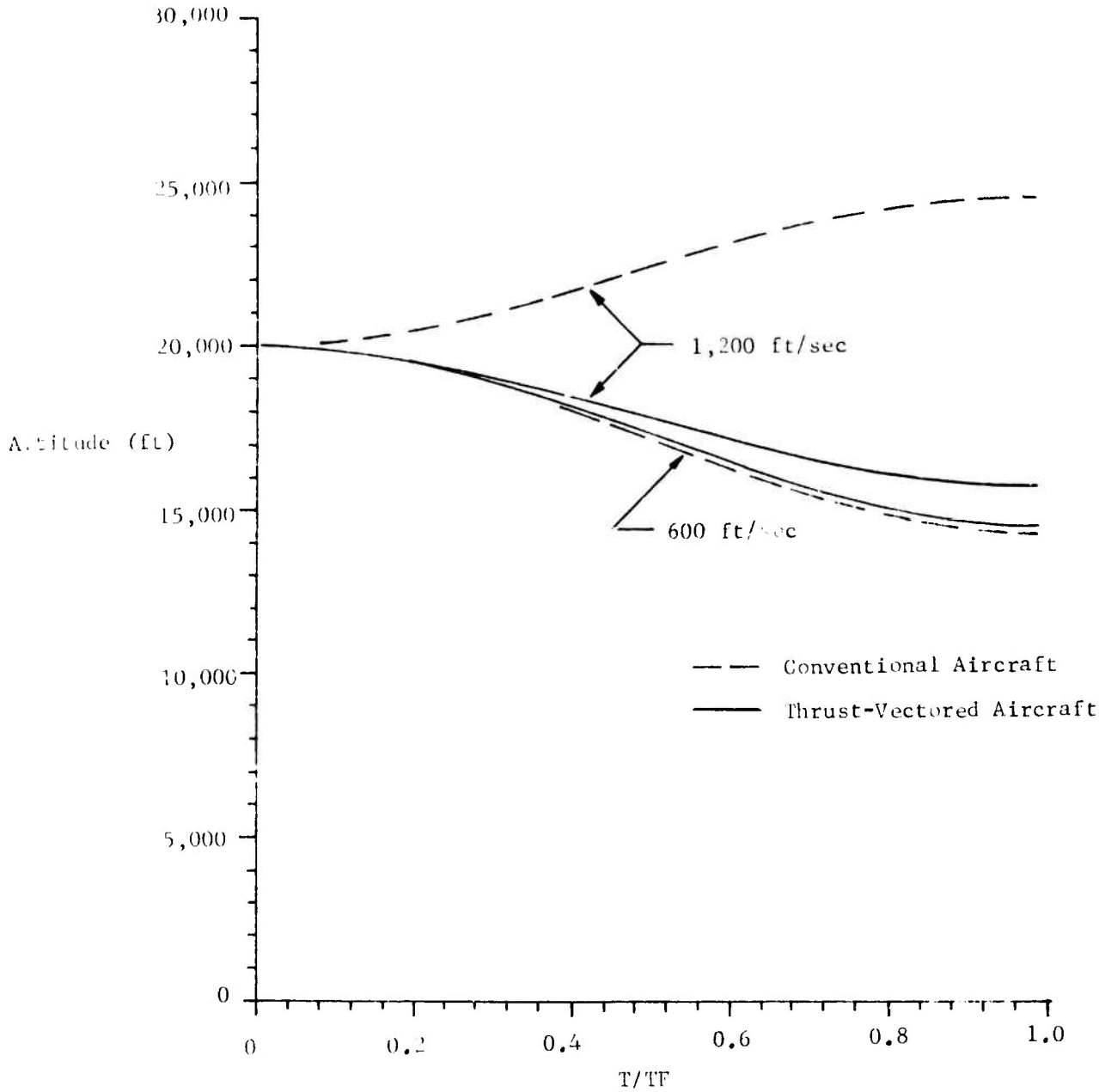

Figure 4. Altitude Profile-Effect of Initial Velocity

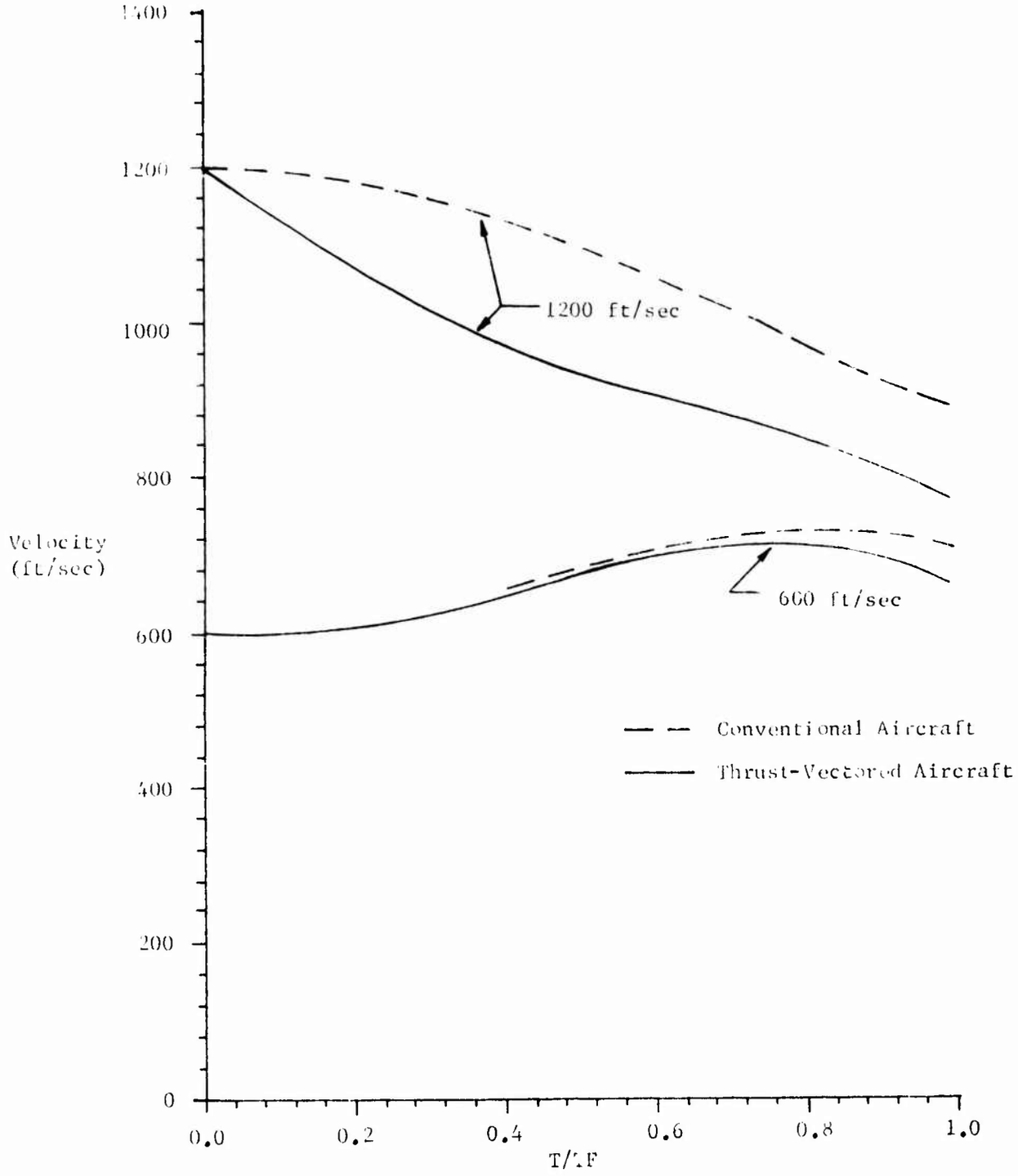

Figure 5. Velocity Profile-Effect of Initial Velocity

In all cases the optimal maneuver moved the velocity toward the corner velocity (corner velocity varies with altitude). Above the corner velocity, the conventional aircraft climbs to lose speed while the thrust-vectored aircraft uses the angle of the thrust vector to lose speed and to tighten up the turn. In all cases the final angle for the thrust vector was about 90° (Figure 6). This was probably due to the requirement that the final flight path angle be zero. In Figure 6 the difference in the bank angle plots for the conventional aircraft at 600 ft/sec and the thrust-vectored aircraft could not be plotted. The optimal bank angle history for a conventional aircraft below the corner velocity agrees well with the procedure which is currently in use for making maximum rate 180° turns in the F-4.

The angle of attack for maximum C_L is about 22°. Therefore, a thrust angle of 36° indicates that the thrust line is 14° above the aircraft axis. Thrust angles for the runs below the corner velocity were small except for the last 30% of the run where only a few degrees of heading change is accomplished and the emphasis is on getting the flight path angle back to zero. For the high speed runs the thrust angle starts out at about 150° to reduce speed and tighten the turn. For the high speed runs the bank angle was considerably higher for the thrust-vectored aircraft, thus increasing turn rate. For the conventional aircraft the bank angle was low for the first part of the turn because of the need to gain altitude to lose air speed (Figure 6).

Weight Penalty. To determine the effect of the added weight which would be required to mechanize the thrust vectoring, runs were made for initial velocities of 600 ft/sec and 1200 ft/sec adding increments of 2000 lbf of weight until the weight was 50,000 lbf. This represents a 25% increase in weight. Considering the capability for aligning the aircraft that exists in the thrust-vectored aircraft, the thrust-vectored aircraft has a combat advantage even up to a 25% weight penalty. The bank angle and thrust angle histories do not change much over the 10,000 lbf range of weights (Figure 10 and Figure 14). Table IV shows the positions of all aircraft at the end of the turn for the 40,000 lbf thrust-vectored aircraft.

For the 600 ft/sec case, the thrust-vectored aircraft with a weight penalty of 2,000 to 10,000 pounds was behind, below, and within 1725 feet of the conventional aircraft (Figure 7, Figure 8, and Table IV). This is well within gun range for a 20 mm gun and the thrust-vectored aircraft is in a position to bring guns to bear. As the weight penalty was increased, the final velocity increased so that for a 6,000 pound penalty the final velocity of the thrust-vectored aircraft was within 1 ft/sec of the conventional aircraft velocity (Table IV). There is no doubt that the thrust-vectored aircraft has the combat advantage. In reading Figures 8, 9, and 10, remember that the final time for each run plotted is different, so a value of T/TF = 1 represents a different time for each run. See Table II for the final time for each run. Figure 10 shows that the bank angle and thrust angle vary only slightly from the 40,000 pound aircraft to the 50,000 pound aircraft.

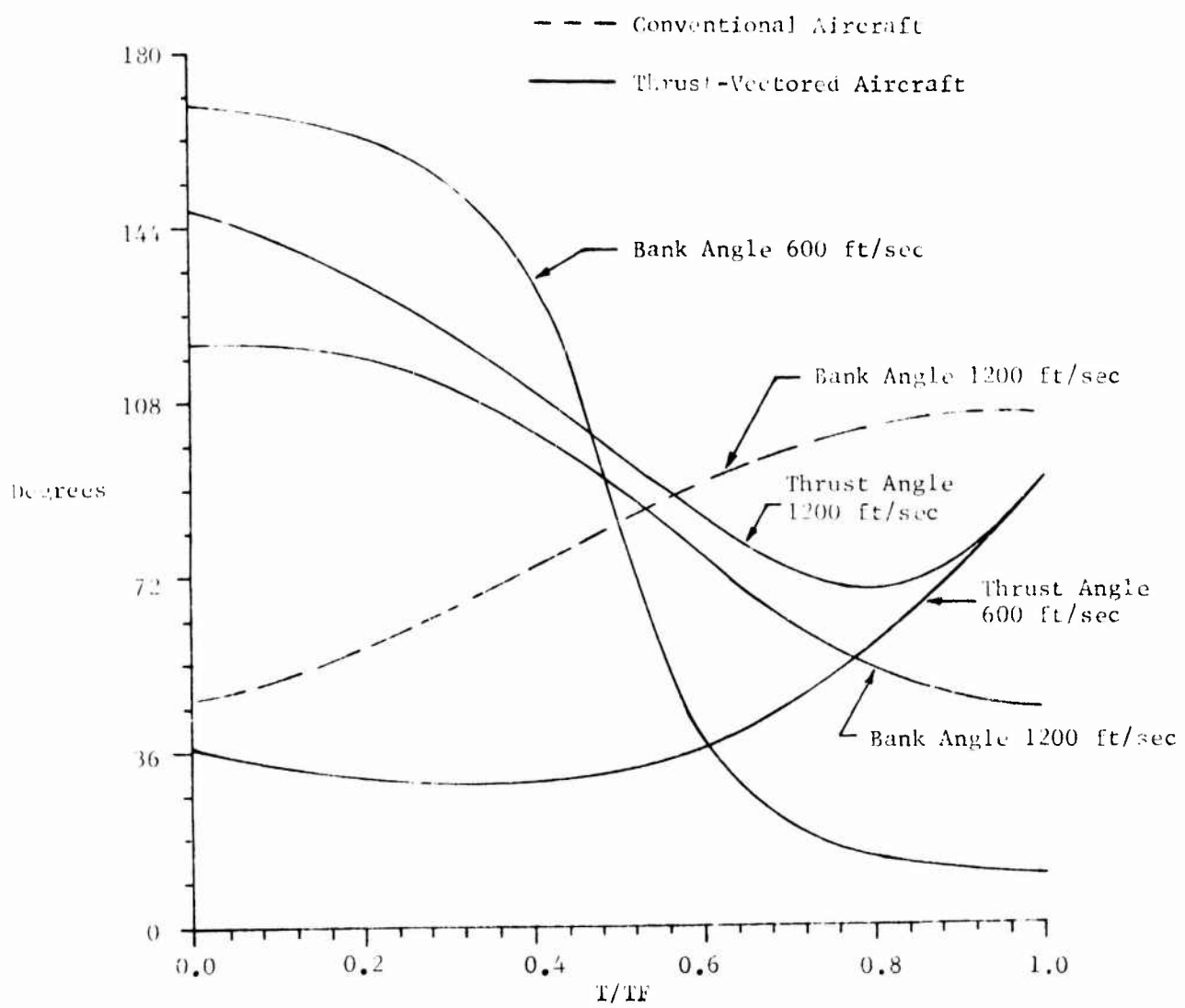

Figure 6. Control History-Effect of Initial Velocity

RUN	INITIAL VELOCITY	C OR TV	WEIGHT	TIME	POSITION AT TIME GIVEN					SLANT RANGE
					t	x	y	ALTITUDE	VELOCITY	
13	600	C	40000	13.13	179	- 402	1264	14398	717	
14		TV	40000		180	- 412	1221	14547	662	157
15		TV	42000		179	- 273	1079	14272	679	340
16		TV	44000		178	- 20	1033	14045	701	660
17		TV	46000		178	223	949	13859	716	976
18	↓	TV	48000	↓	178	635	905	13700	732	1402
19	600	TV	50000	13.13	177	930	878	13560	745	1725
20	1200	C	40000	13.16	167	3131	8344	24468	910	
21		TV	40000		180	1793	6310	24526	699	2435
22		TV	42000		177	1975	6592	24539	707	2100
23		TV	44000		173	2170	6886	24509	722	1747
24		TV	46000		170	2382	7135	24486	740	1422
25	↓	TV	48000	↓	165	2606	7394	24407	745	1087
26	1200	TV	50000	13.16	162	2784	7521	24361	749	900

TABLE IV. Position at the End of 180° Turn for One Thrust-Vectored Aircraft Effect of Weight Penalty

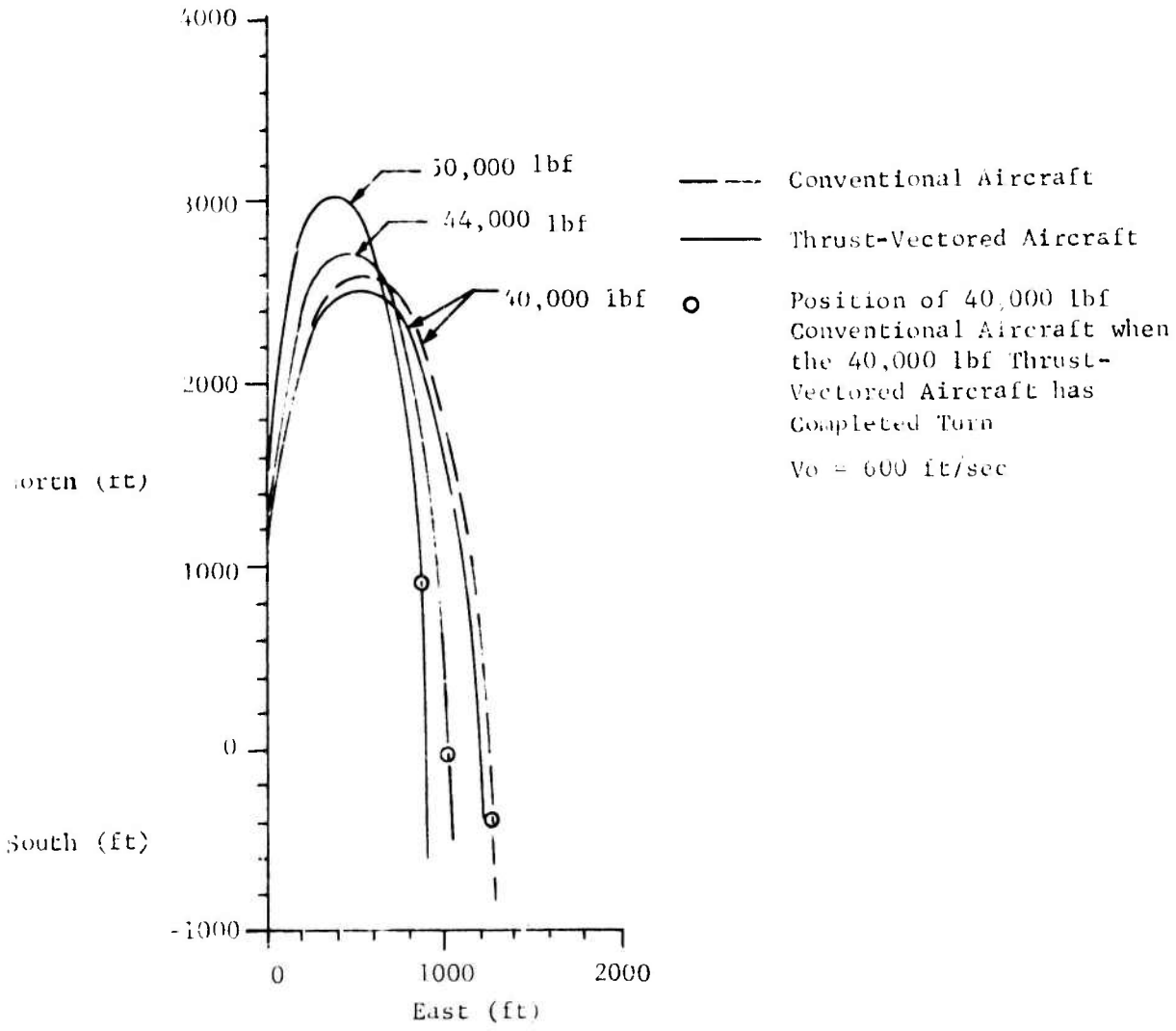

Figure 7. Ground Trace-Effect of Weight Penalty

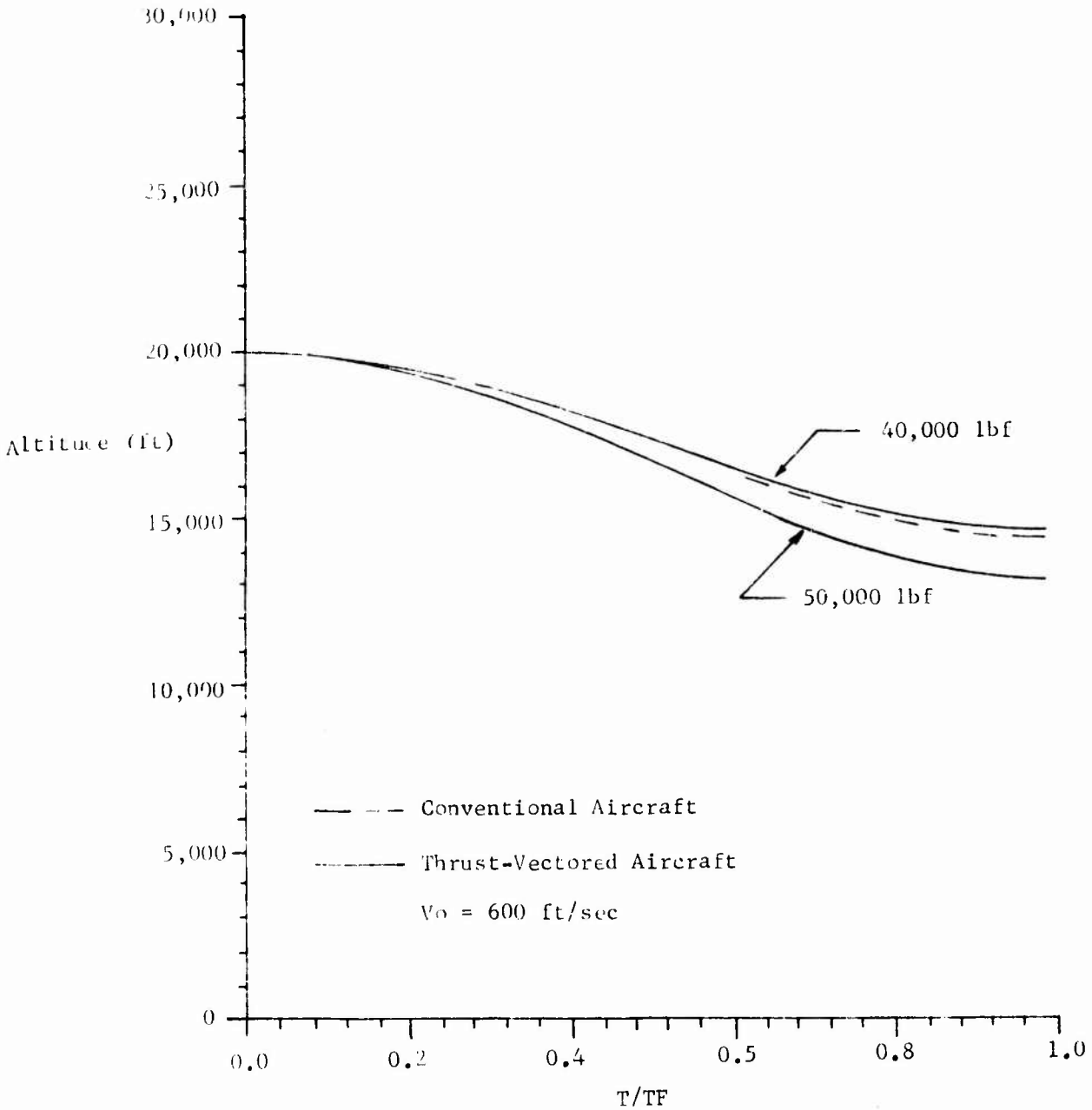

Figure 8. Altitude Profile-Effect of Weight Penalty

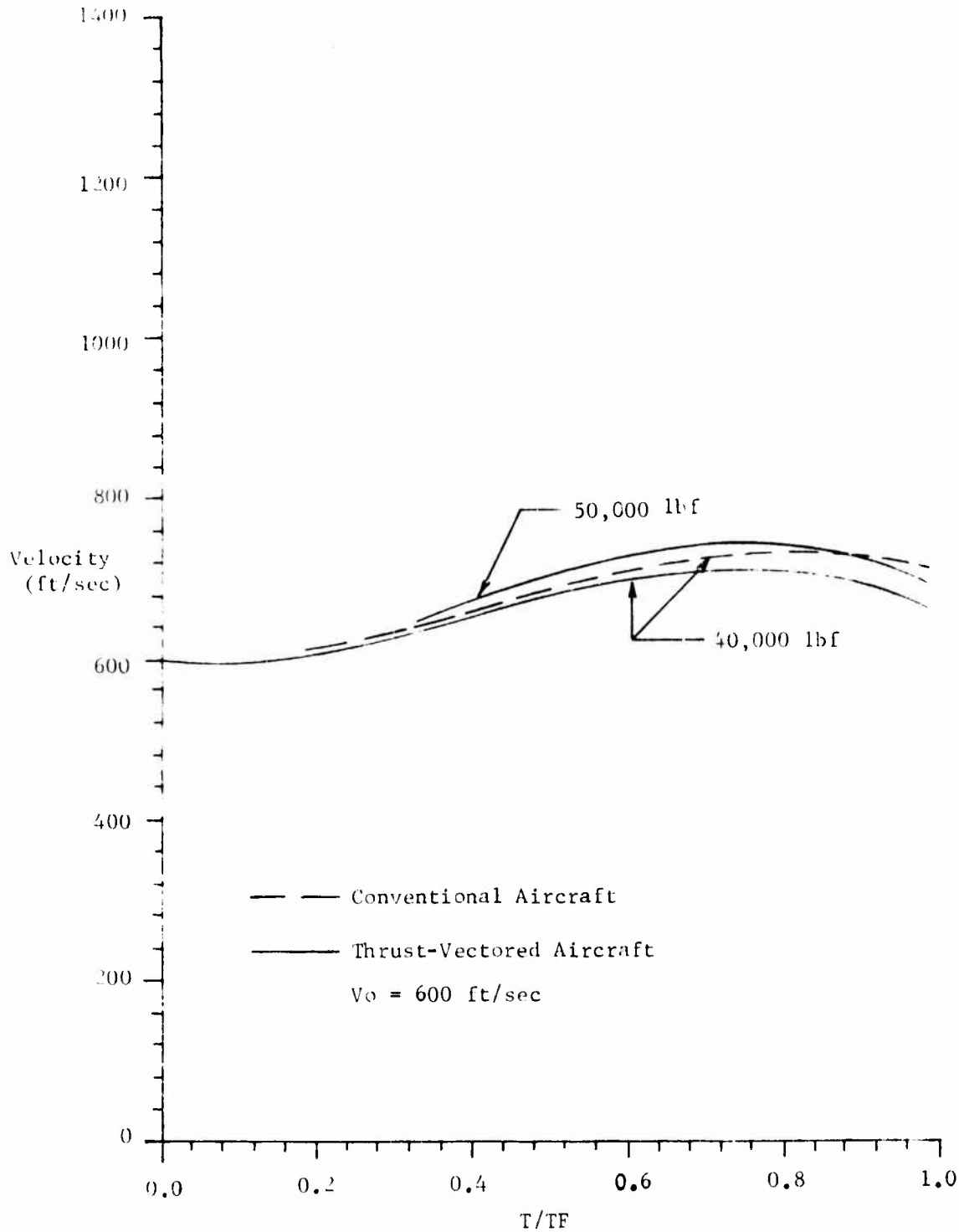

Figure 9. Velocity Profile-Effect of Weight Penalty

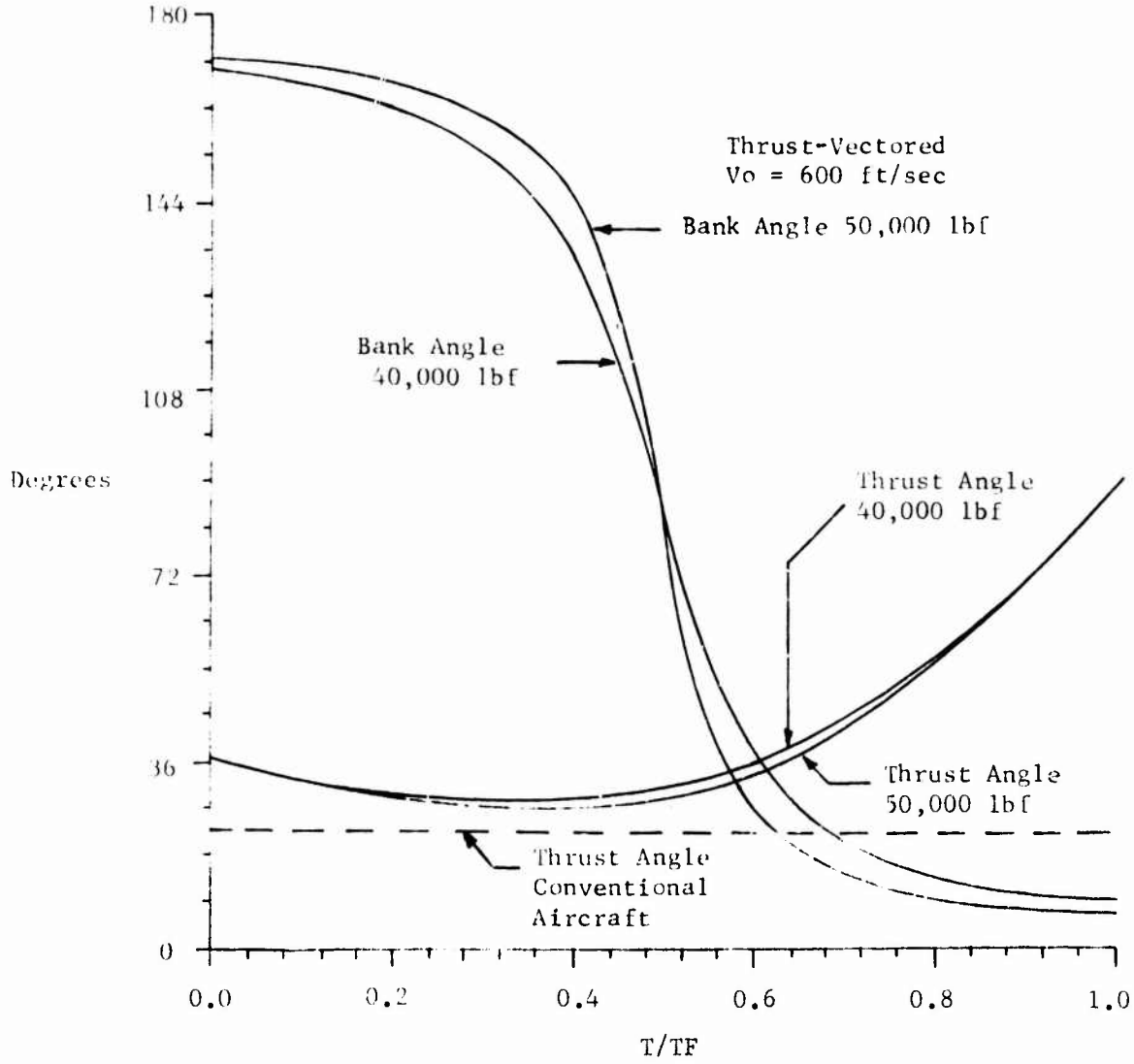

Figure 10. Control History-Effect of Weight Penalty

For the 1200 ft/sec run, it was necessary to constrain the final altitude to be the altitude of the conventional aircraft. Otherwise, there was too great a difference in the final altitudes to be able to determine which aircraft had an advantage (see Figure 4). For all weights, the thrust-vectored aircraft was inside and in front of the conventional aircraft. The thrust-vectored aircraft was slower and within 110 ft of the altitude of the conventional aircraft. Since the thrust-vectored aircraft is slower, a turn toward the conventional aircraft would tend to put the thrust-vectored aircraft behind the conventional aircraft. With the computer program used, it was not possible to pursue this tactic to determine which aircraft has the advantage.

Table IV shows the positions of all aircraft at the end of the turn for the 40,000 lbf thrust-vectored aircraft. Since the altitude is almost the same for all aircraft, Figure 11 and Figure 12 give a very good picture of the relative position of each aircraft in space. Constraining the final altitude of the thrust-vectored aircraft resulted in almost no difference in the altitude profiles for the thrust-vectored aircraft of different weights. The difference in velocity between the conventional and the thrust-vectored aircraft makes it difficult to predict times and trajectories for a turn into the conventional aircraft if the conventional aircraft continues the turn. Figure 13 shows that the velocity of the thrust-vectored aircraft does not change much with weight. However, the slant ranges (Table IV) are such that if the conventional aircraft tries to turn away from the thrust-vectored aircraft, the thrust-vectored aircraft will have the advantage. For 1200 ft/sec initial velocity (Figure 14), there is a slightly greater variation in bank angle with weight in comparison to the same variation at 600 ft/sec initial velocity (Figure 10).

The effect of weight penalty on the x direction position at 13.13 seconds for the low speed runs and 13.16 seconds for the high speed runs was to make it more positive. Since the low speed thrust-vectored aircraft was behind the conventional aircraft, the slant range was increased with weight penalty; and because for the high speed runs the thrust-vectored aircraft was in front, the slant range decreased with weight penalty. If the final altitude of the low speed runs had been constrained, increased weight would have produced wider turns, thus duplicating the effect of weight on the high speed runs (Figure 7 and Figure 11). Most of the effect of a constraint on the final altitude is on the y direction position since it tends to tip the plane of the turn up or down, rotating it about the x axis. There is very little effect on the x position, and the effect of increased weight on final x direction position (more negative) is the same for both speed regions.

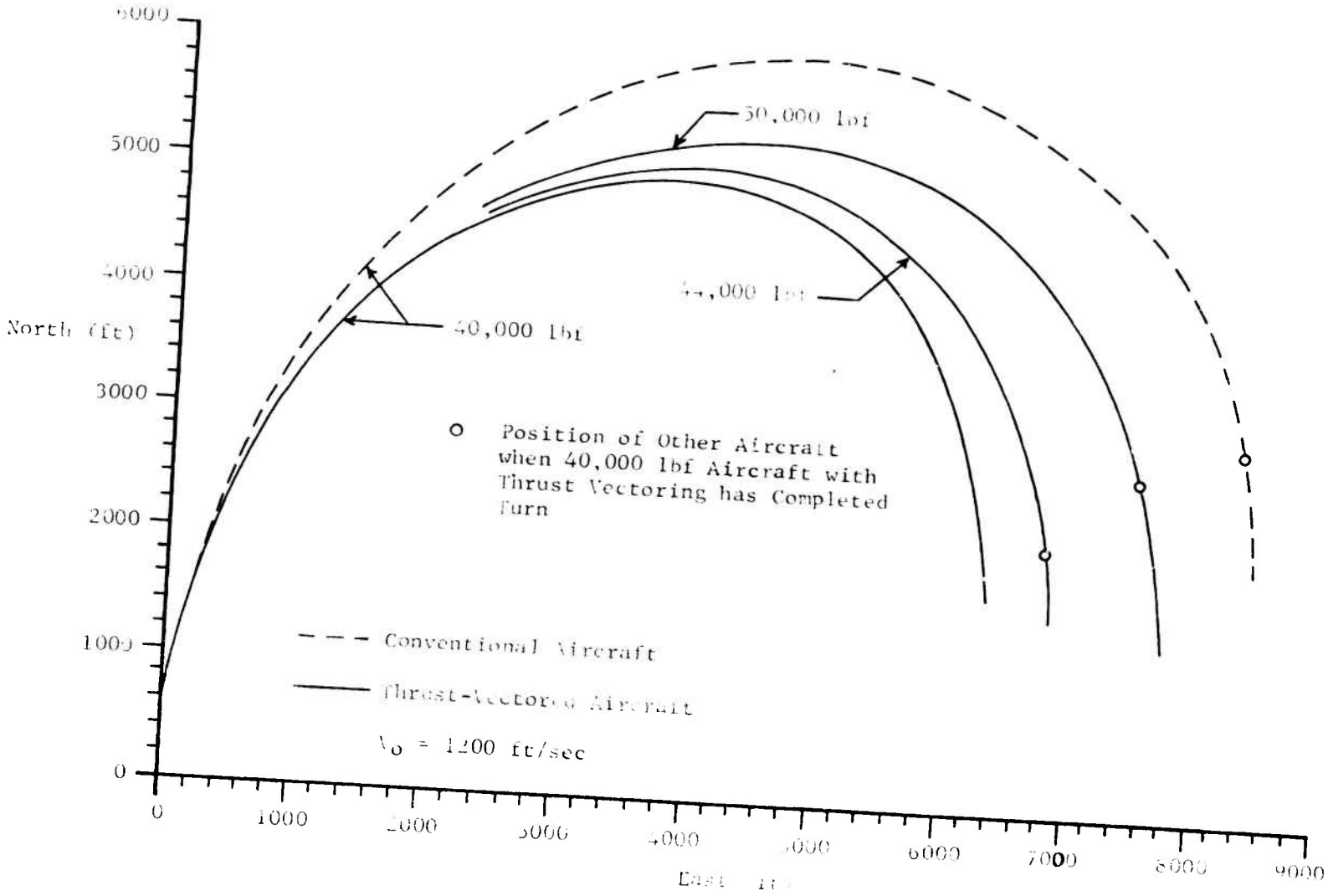

Figure 11. Ground Trace-Effect of Weight Penalty

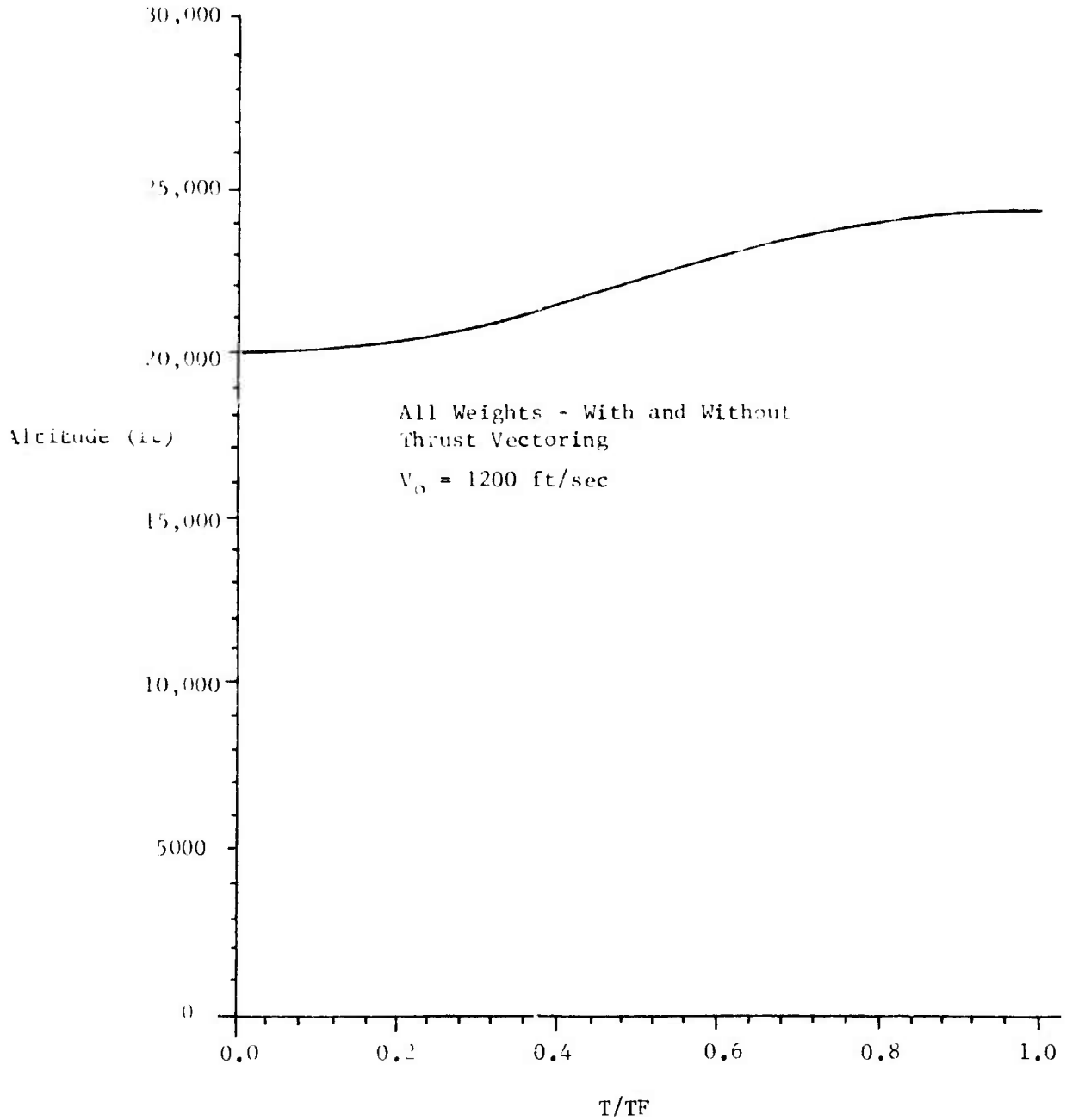

Figure 12. Altitude Profile-Effect of Weight Penalty

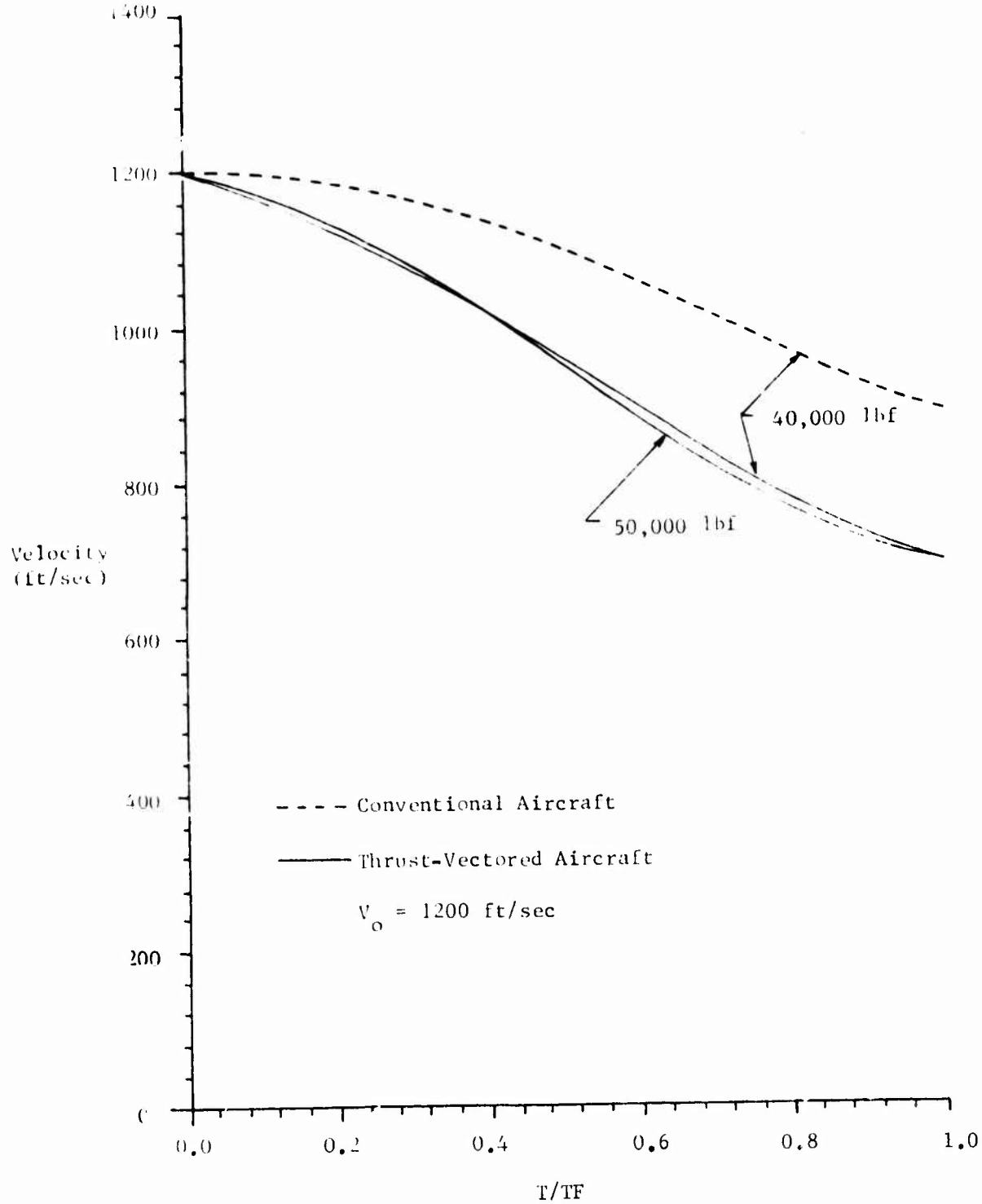

Figure 13. Velocity Profile-Effect of Weight Penalty

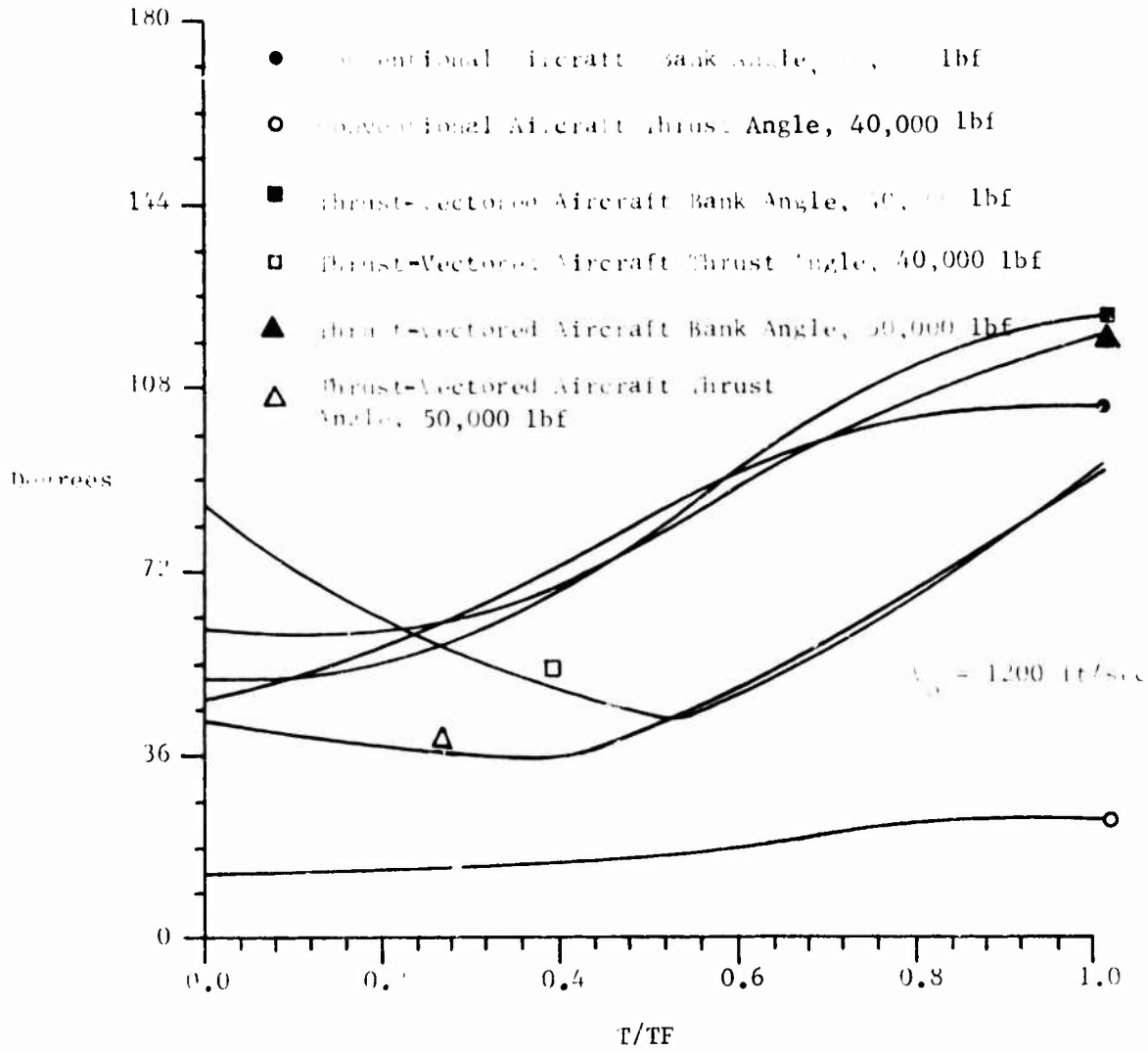

Figure 14. Control History-Effect of Weight Penalty

Thrust-to-Weight. Several values of initial thrust-to-weight ratios were investigated. These ranged from 0.585 to 1.5. The lower value was determined by basic aircraft data. For the case of 600 ft/sec initial velocity, the thrust-vectored aircraft was slower, above, inside, and in front of their conventional counterparts. As long as the turn was continued, the conventional aircraft could not point at the thrust-vectored aircraft. The slant range varied from 157 ft at T/W = 0.585 up to 614 ft at T/W = 1.5, and for the higher thrust-to-weight ratios the major portion of the slant range was altitude. Being above and slower, the thrust-vectored aircraft probably has an advantage. The track over the ground (Figure 15 and Figure 16) and the altitude (Figure 17) are not greatly affected by thrust-to-weight ratio in the low speed region. There is a noticable effect on the velocity profile (Figure 18), but the conventional aircraft is more affected by thrust-to-weight ratio than the thrust-vectored aircraft. The effect is to increase the velocity difference between the conventional aircraft and the thrust-vectored aircraft as thrust-to-weight ratio increases. Figures 19 and 23 show that the control histories are not changed greatly by thrust-to-weight ratio, although the effect is greatest on bank angle at initial velocities above the corner velocity. This is probably due to the effect of constraining the final altitude.

As with the weight penalty investigation, it was necessary to constrain the final altitude for the cases above the corner velocity. For an initial velocity of 1200 ft/sec, the thrust-vectored aircraft was slower, above, inside, and in front of their conventional counterparts. The large slant ranges involved make an evaluation of advantage difficult. In Figure 20 the ground trace for the conventional aircraft with T/W = 1.5 crosses inside of the trace for the conventional aircraft with T/W = 1.09. This is due to the fact that with greater thrust, the first aircraft must climb higher faster to reduce velocity to the corner velocity (Figure 21). The same thing is true for the thrust-vectored aircraft. Thrust-to-weight ratio does not have much effect on the velocity profile of the thrust-vectored aircraft for the high speed region (Figure 22). Since increased thrust-to-weight ratio increases the velocity for the conventional aircraft, it increases the velocity difference between the conventional and the thrust-vectored aircraft. The effect of thrust-to-weight ratio on the thrust angle was small. The effect on bank angle was significant (Figure 23). As thrust-to-weight ratio was increased, the initial bank angle decreased and final bank angle increased, the initial bank angle decreased and final bank angle increased for both the thrust-vectored and the conventional aircraft. The change was greatest for the thrust-vectored aircraft.

In both speed regions the effect of increasing thrust-to-weight ratio was to make the x direction more positive, the y direction position smaller, and the slant range greater (Table V). In the low speed region increasing thrust-to-weight ratio reduced the time for the turn and increased final velocity, but in the high speed region there was a negligible effect on turn time and final velocity. For both regions the velocity difference between the conventional and the thrust-vectored aircraft increased with increasing thrust-to-weight ratio.

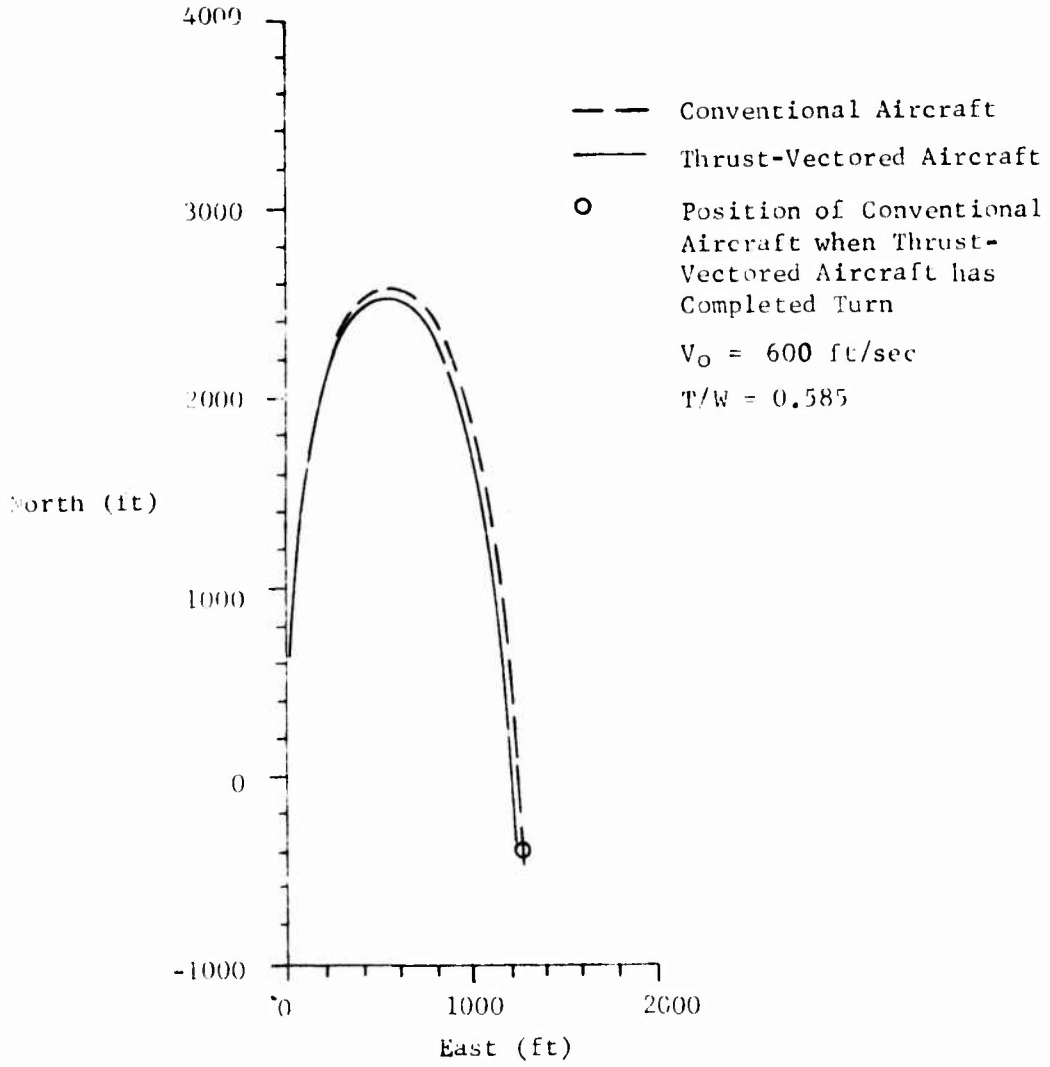

Figure 15. Ground Trace-Effect of Thrust-to-Weight Ratio

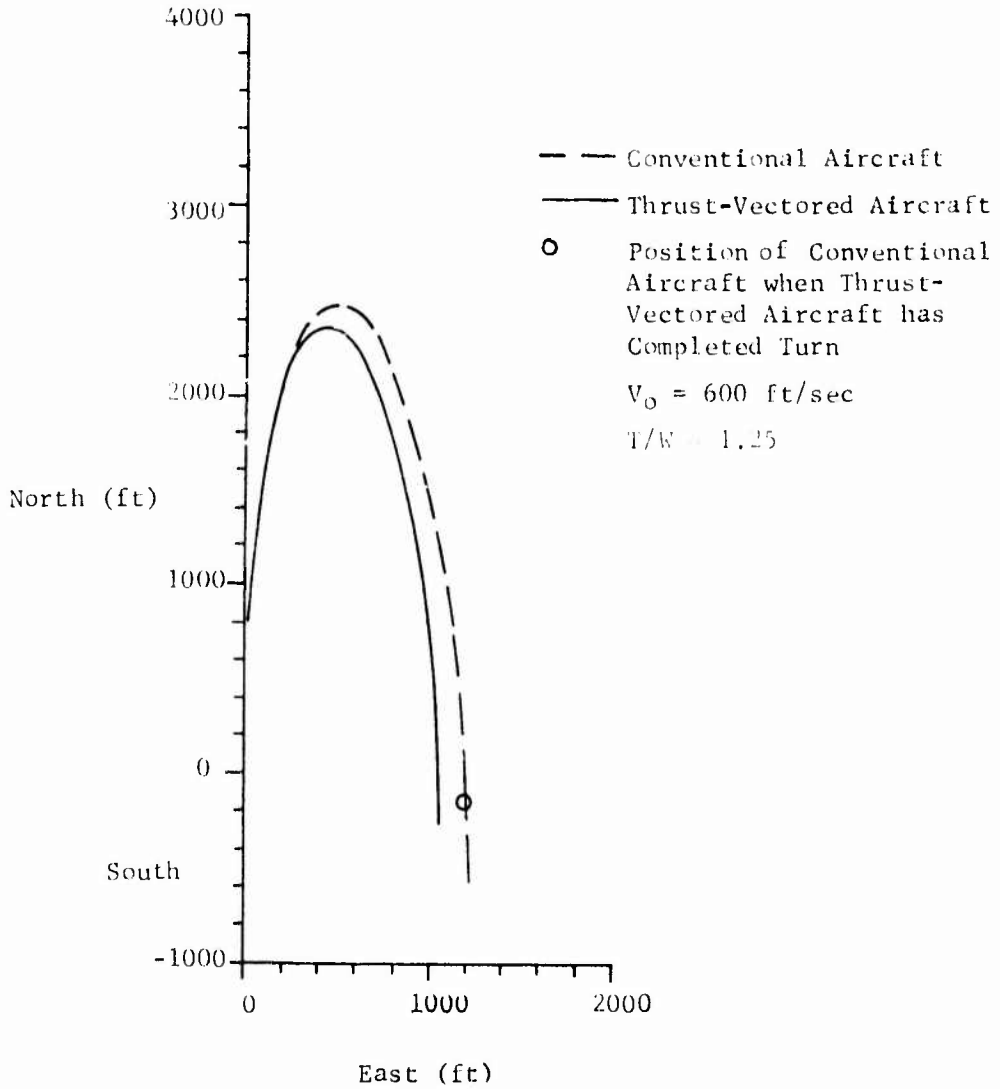

Figure 16. Ground Trace-Effect of Thrust-to-Weight Ratio

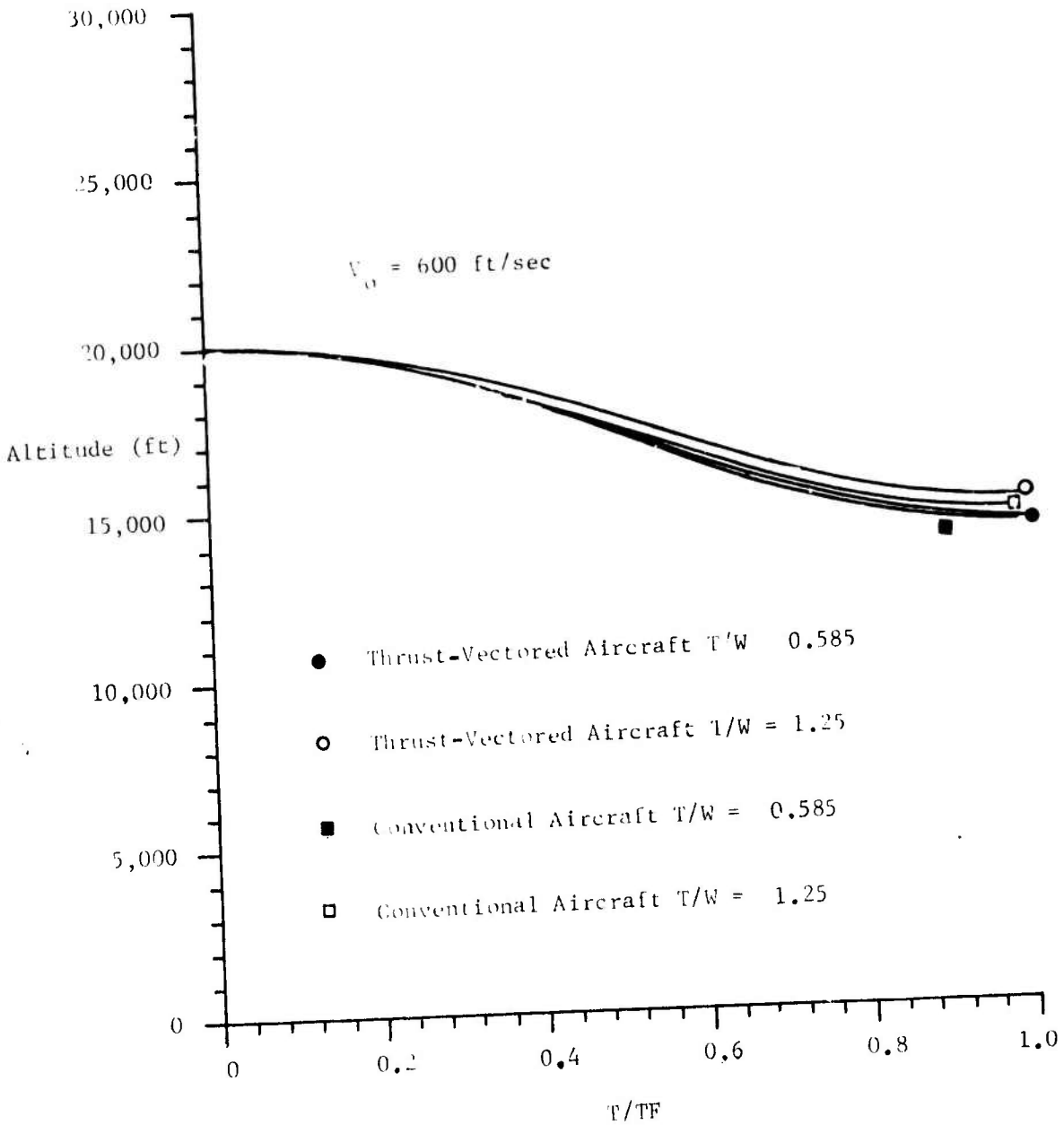

Figure 17. Altitude Profile-Effect of Thrust-to-Weight Ratio

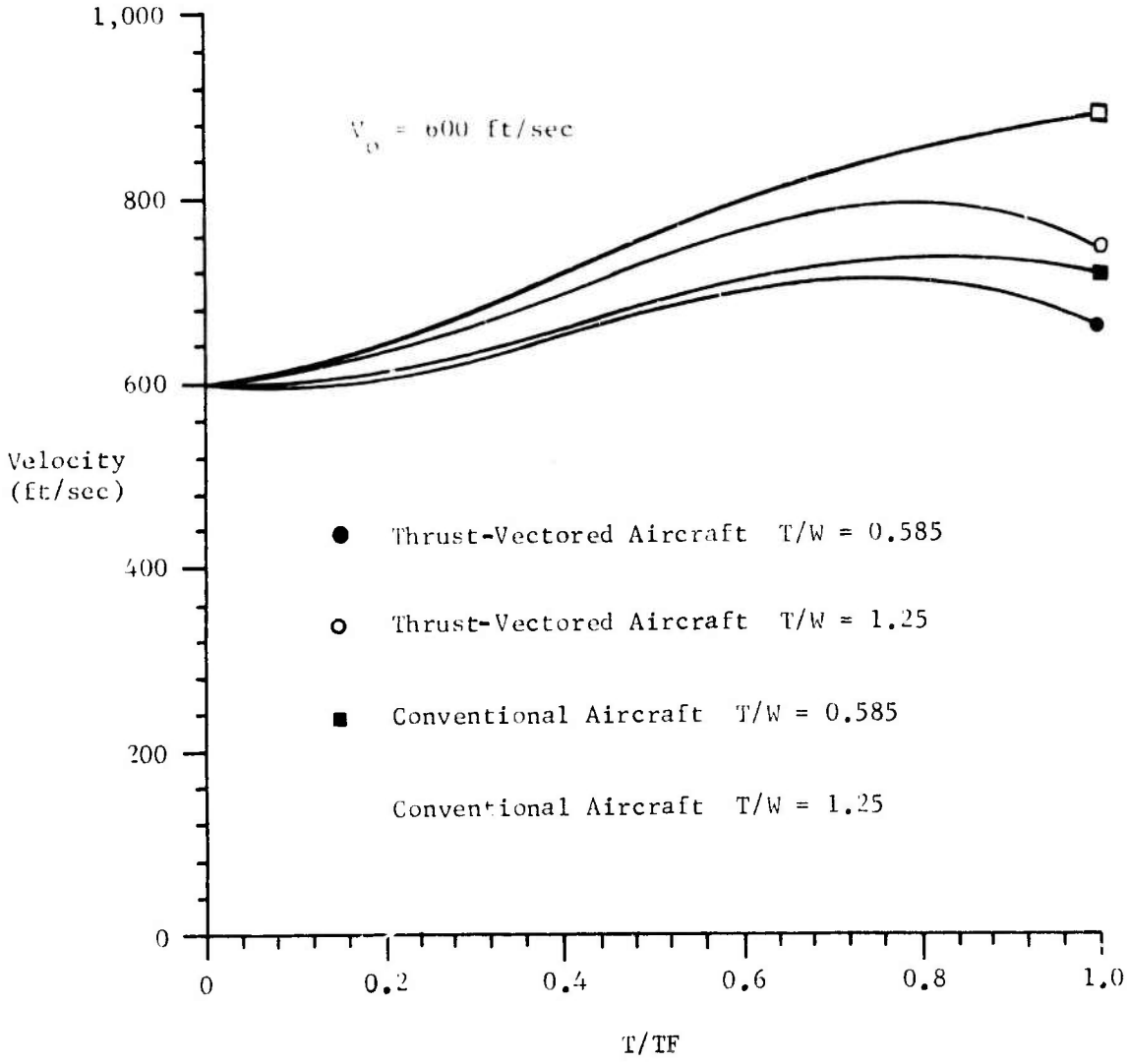

Figure 18. Velocity Profile-Effect of Thrust-to-Weight Ratio.

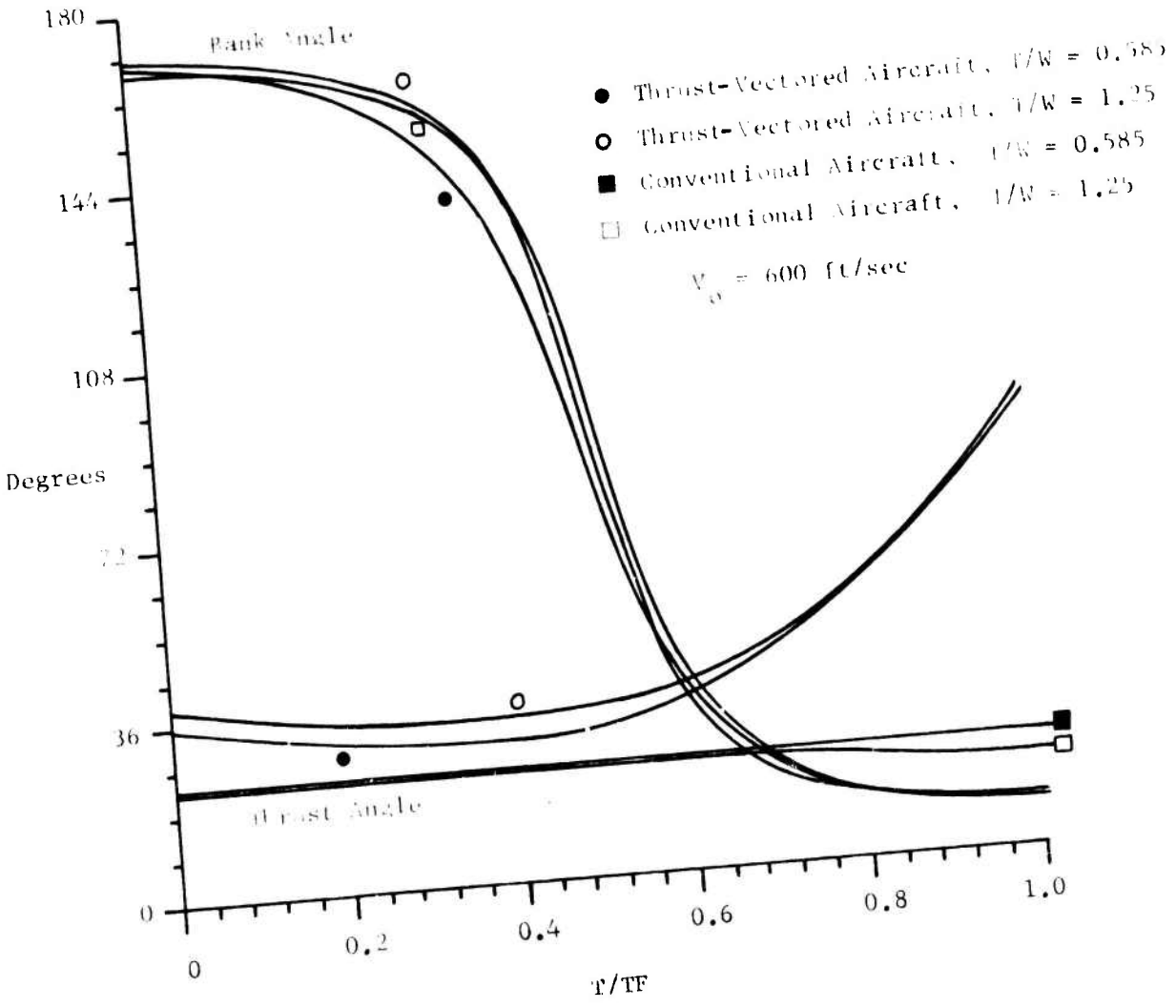

Figure 19. Control History-Effect of Thrust-to-Weight Ratio

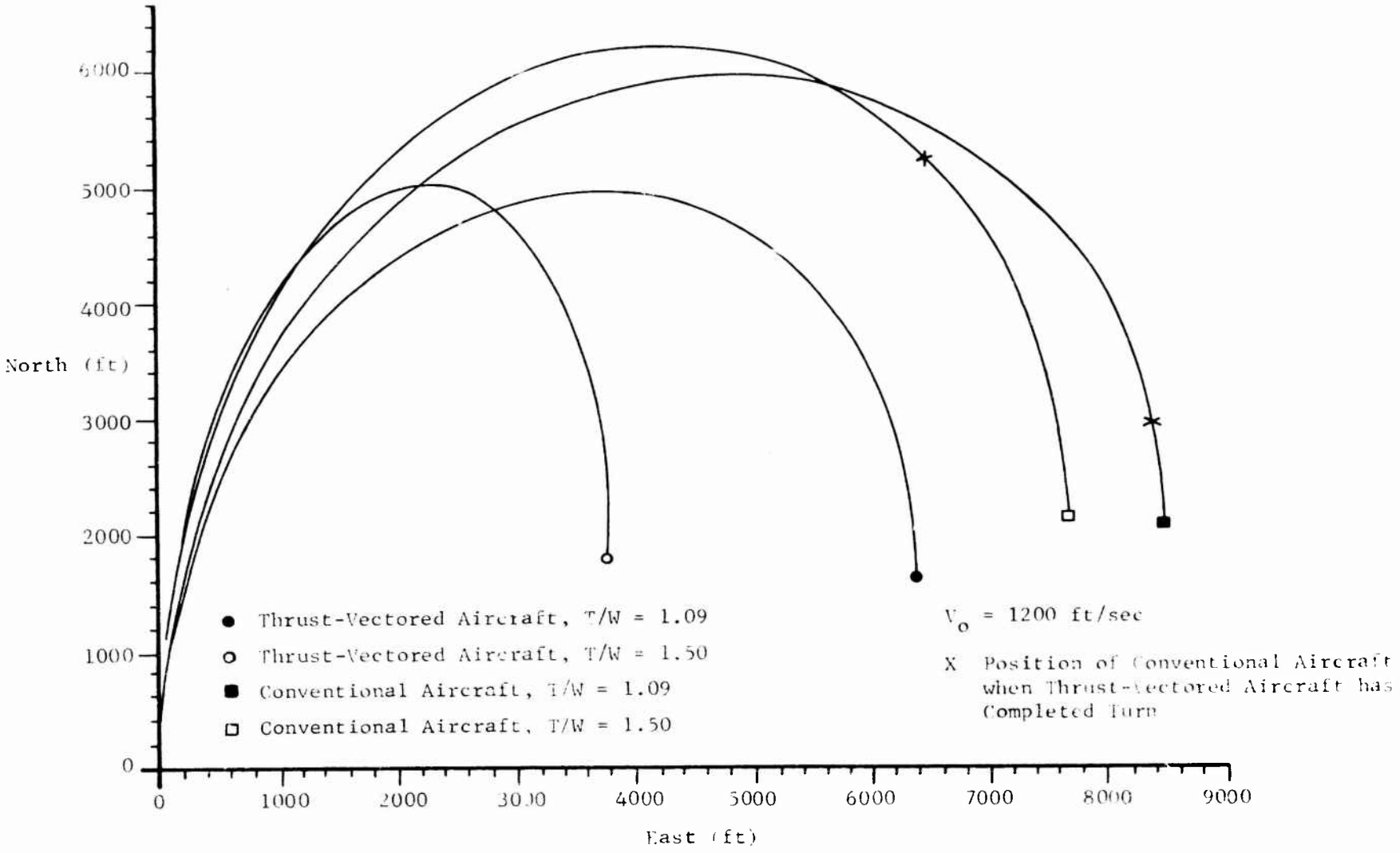

Figure 20. Ground Trace-Effect of Thrust-to-Weight Ratio

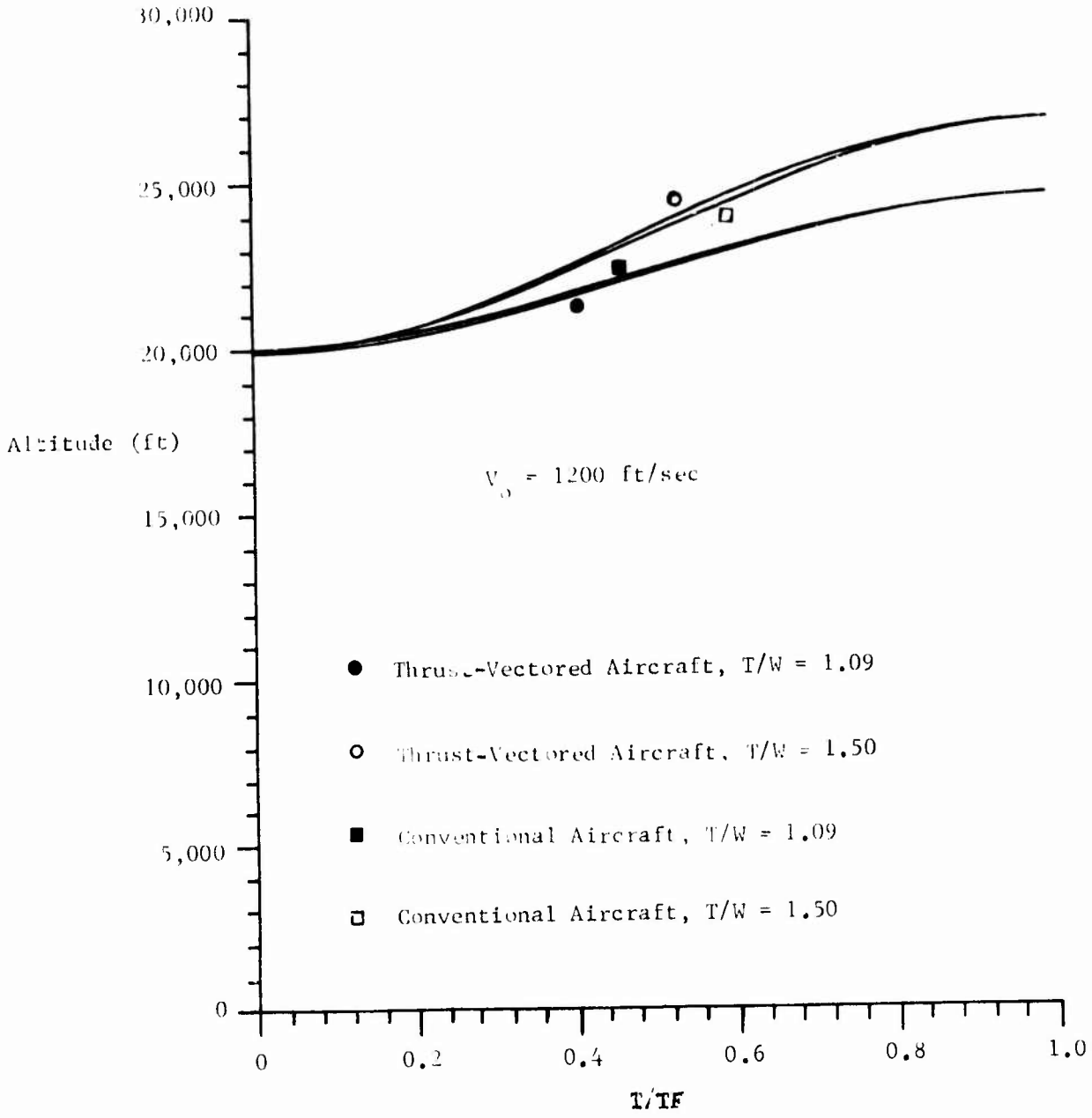

Figure 21. Altitude Profile-Effect of Thrust-to-Weight Ratio

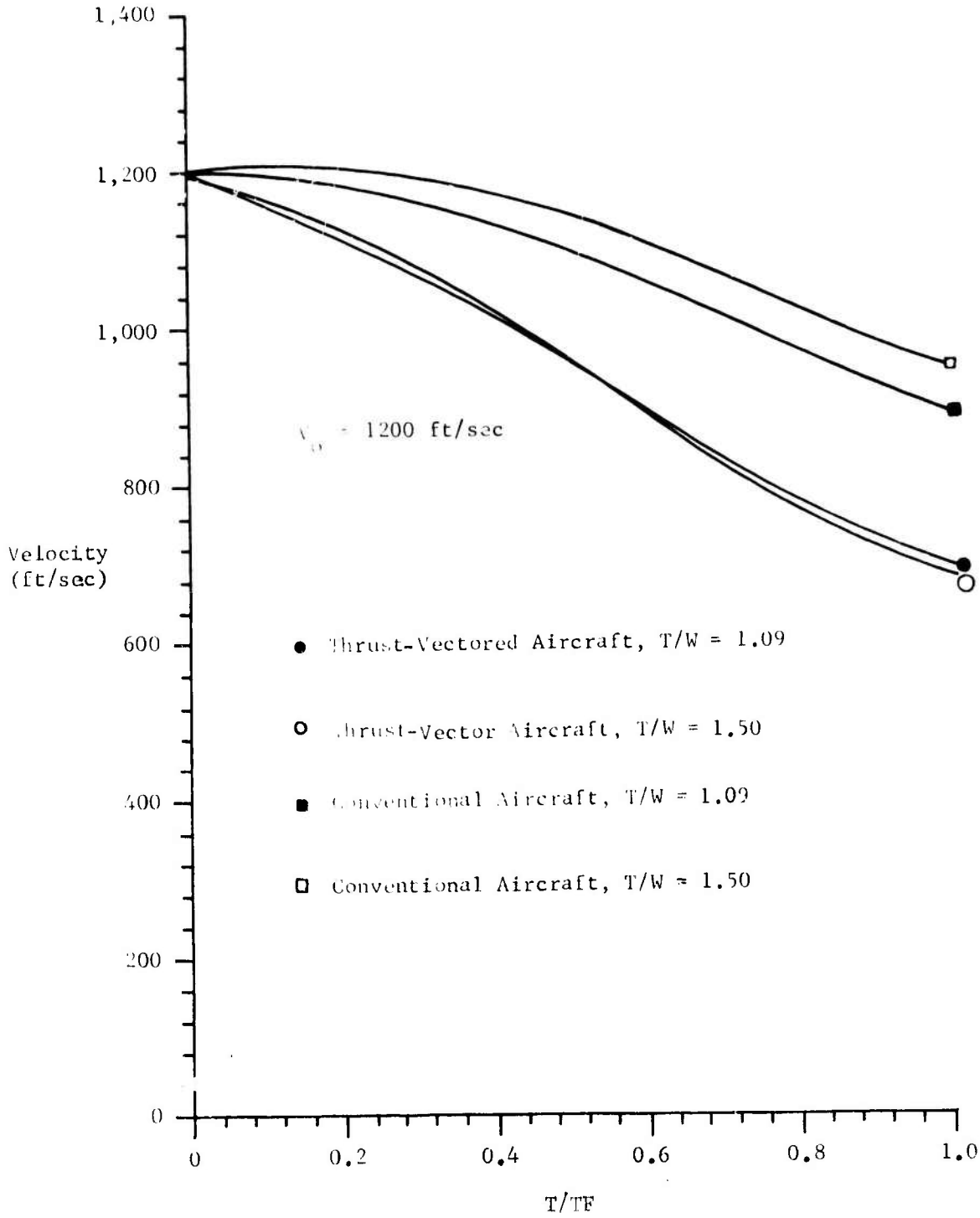

Figure 22. Velocity Profile-Effect of Thrust-to-Weight Ratio

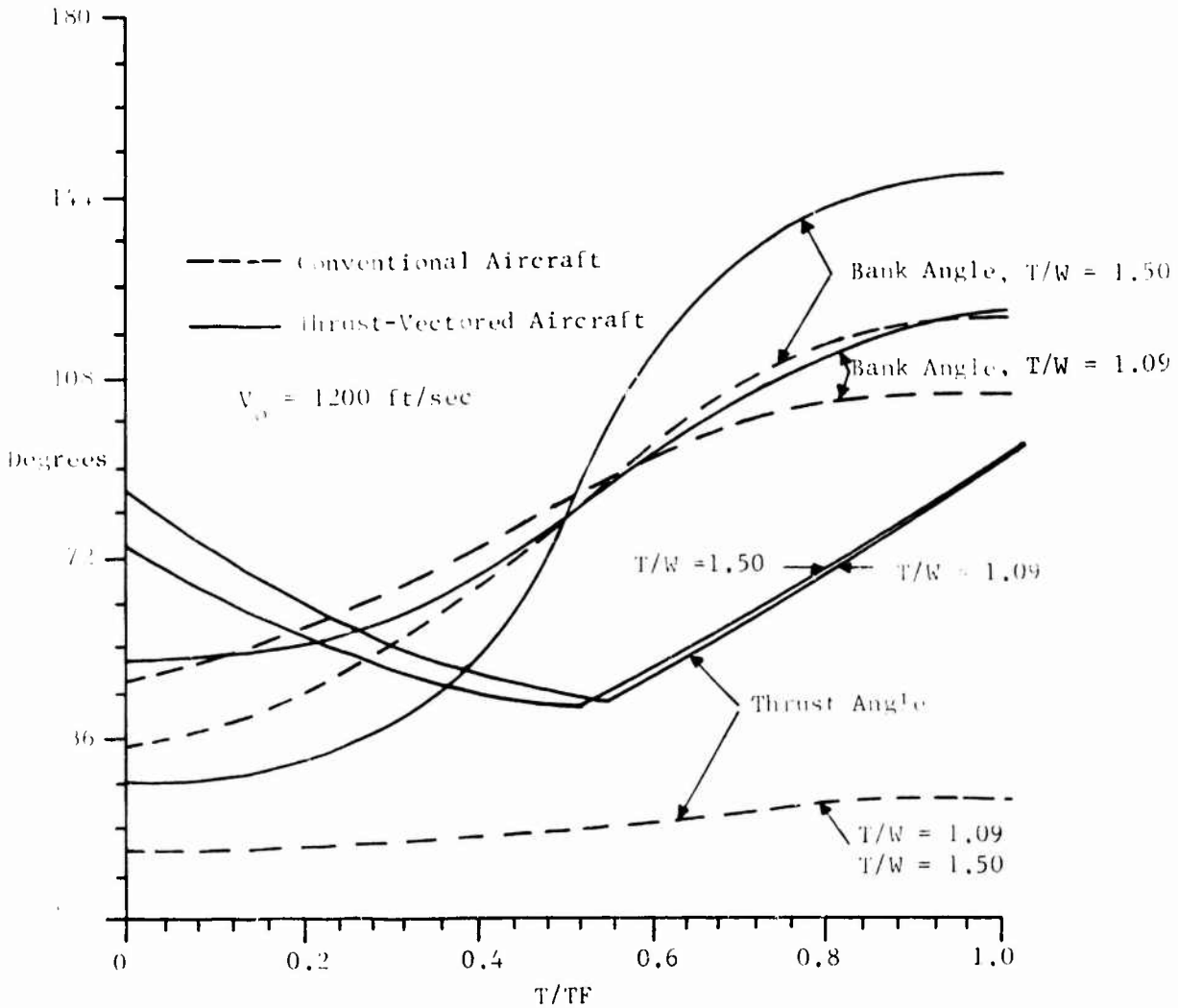

Figure 23. Control History-Effect of Thrust-to-Weight Ratio

RUN	INITIAL VELOCITY	C OR TV	T/W AT 20,000 FT	TIME	POSITION AT TIME GIVEN					SLANT RANGE
					ζ	x	y	ALTITUDE	VELOCITY	
27	600	C	0.585	13.13	179	- 402	1264	14398	717	
28		TV	0.585	13.13	180	- 412	1221	14547	662	157
29		C	0.750	12.57	179	- 297	1158	14459	755	
30		TV	0.750	12.57	180	- 360	1122	14648	685	202
31		C	1.000	11.78	178	- 248	1120	14557	808	
32		TV	1.000	11.78	180	- 298	1107	14818	715	266
33		C	1.250	11.13	176	- 160	1205	14604	882	
34		TV	1.250	11.13	180	- 254	1057	14967	741	403
35		C	1.500	10.57	176	- 78	1206	14555	967	
36	600	TV	1.500	10.57	180	- 222	1012	15120	760	614
37	1200	C	1.092	13.16	167	3131	8344	24468	910	
38		TV	1.092	13.16	180	1793	6310	24526	695	2435
39		C	1.250	13.22	168	3212	7843	25581	919	
40		TV	1.250	13.22	180	1831	5276	25637	681	2915
41		C	1.500	13.15	165	3493	7458	26695	975	
42	1200	TV	1.500	13.15	180	1882	3734	26804	687	4059

TABLE V. Position at the End of 180° Turn for Thrust-Vectored Aircraft
Effect of Thrust-to-Weight Ratio

Figure 28 shows that for the conventional aircraft the turn radius for the T/W = 1.5 aircraft is everywhere greater than for the one with T/W = 1.09. However, for the thrust-vectored aircraft, the additional thrust is used to slew the aircraft down and increase the turn rate. Thus (for a 600 ft/sec initial velocity), the radius of turn for the aircraft with a thrust-to-weight ratio of 1.5 is always less than the turn radius of the aircraft with a lower thrust-to-weight ratio. For a 1200 ft/sec initial velocity, the radius of turn is practically independent of thrust-to-weight ratio.

General. The initial value of excess thrust (gross thrust minus the sum of total aircraft drag and ram drag) is given in Table V. Engine data is given in Reference 4. The data goes up to Mach 1.0 and the Mach numbers for the runs ranged from 0.45 for runs 1 and 2 up to 1.57 for runs 11 and 12. The gross thrust and ram drag figures for the runs with initial velocities of 1200 ft/sec and above may not be completely realisitc. However, Table VI shows that the lowest values of excess thrust do occur in the transonic region as one would expect. Final values of excess thrust ranged from -6085 for run 2 to -48908 for run 11.

All turns were at $C_{L_{max}}$ for the portion of the turn where the velocity was less than the local corner velocity and at maximum g load where the velocity was greater than the local corner velocity. Both the conventional and the thrust-vectored aircraft were on the maximum performance boundary throughout the turn for all conditions.

Figure 24 shows that the flight path angle was almost symmetric about the mid time of the turn. This was probably due to the fact that the initial and final conditions on flight path angle were both zero. For the thrust-vectored aircraft the trends are as expected--the greater the initial velocity, the shallower the angle of descent. The trend for the conventional aircraft is also as expected except for the 1400 ft/sec initial velocity run which had a smaller flight path angle throughout the turn than the 1200 ft/sec initial velocity run. Total angular rate trends (Figure 25) were also as expected with the highest turn rates occurring for initial velocities closest to the corner velocity (800 and 1000 ft/sec) for both conventional and thrust-vectored aircraft. For the thrust-vectored aircraft the runs with initial velocities of 1200 ft/sec and 1400 ft/sec have a higher turn rate over the final portion of the turn where a return to zero flight path angle is the driving factor because with higher excess thrust they are able to maintain a velocity closer to the corner velocity. Over this portion of the turn, flight path angle is being changed significantly but the heading is only being changed 3 or 4 degrees. Since heading is not driving the optimization over this portion of the turn, turn rate drops off.

RUN NUMBERS	INITIAL EXCESS THRUST - lbf	INITIAL VELOCITY ft/sec
1 and 2	5973	400
3 and 4, 13 thru 19, 27 thru 36	- 5199	600
5 and 6	-20934	800
7 and 8	-17179	1000
9 and 10, 20 and 21, 37 thru 42	- 919	1200
11 and 12	11009	1400
22	- 3835	1200
23	- 6893	1200
24	-10092	1200
25	-13435	1200
26	-16919	1200

TABLE VI. Initial Excess Thrust

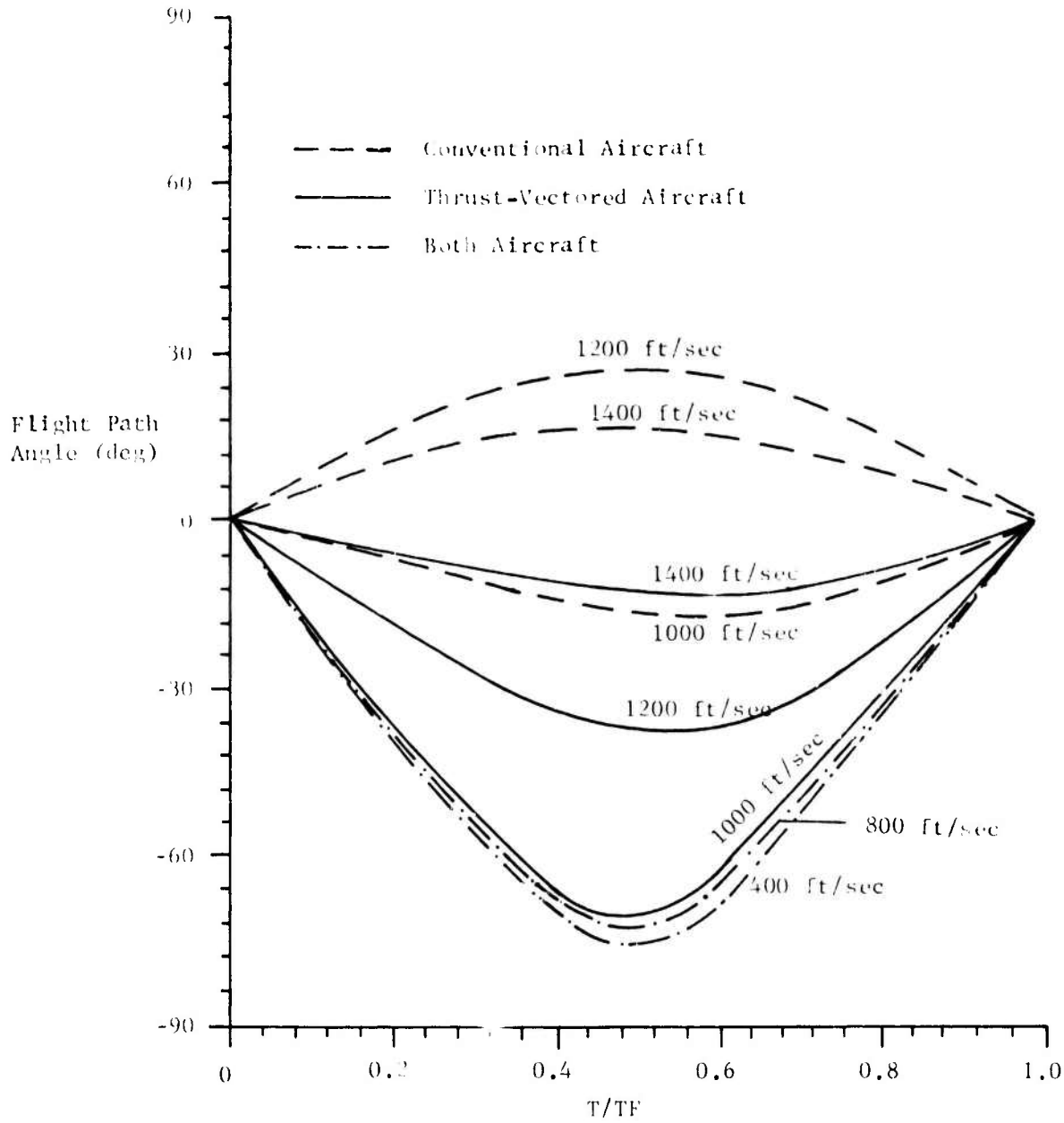

Figure 24. Flight Path Angle-Effect of Initial Velocity

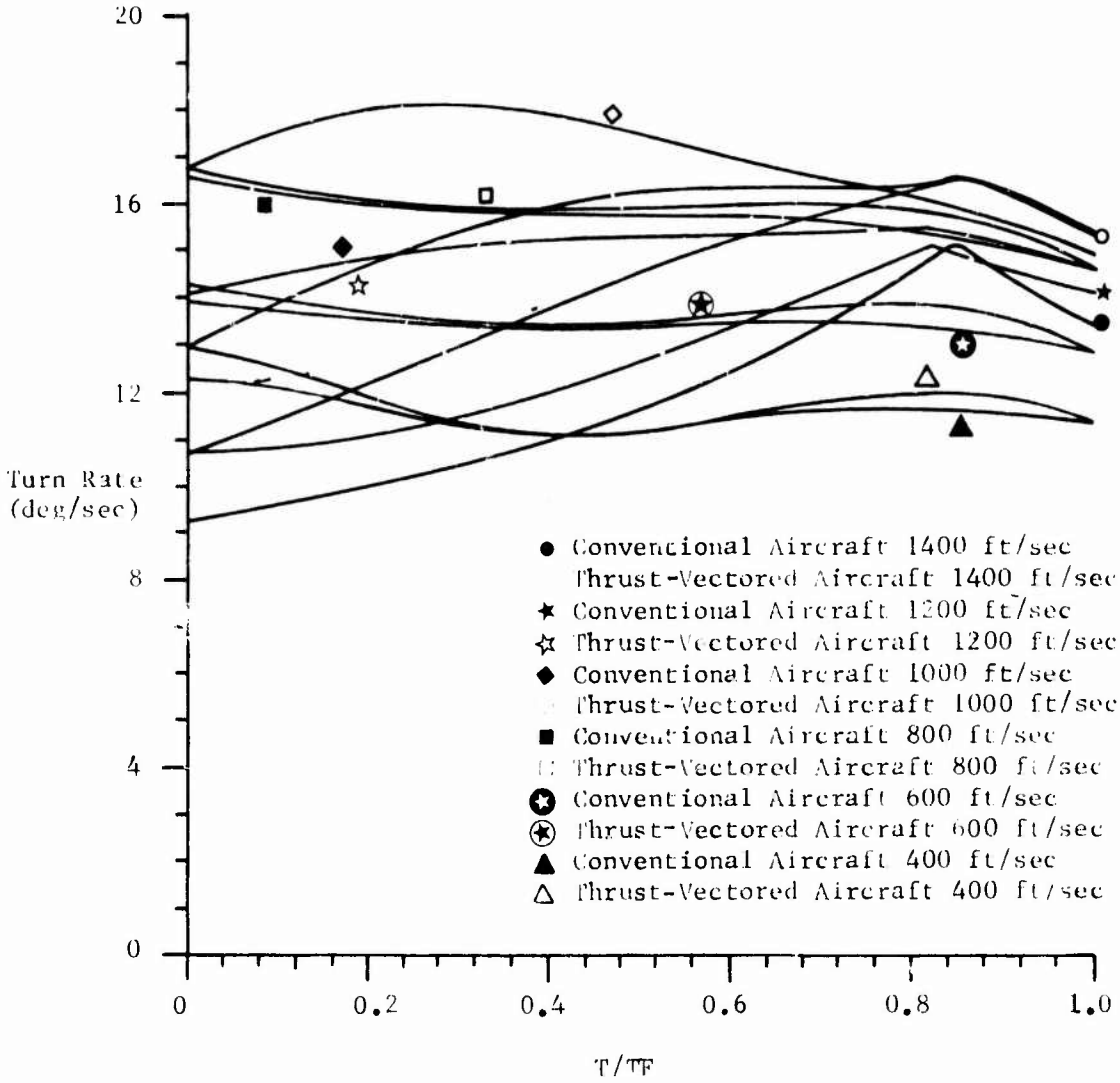

Figure 25. Total Angular Rate-Effect of Initial Velocity

The effect of initial velocity on turn radius was uniform and predictable (Figure 26). The effect of weight penalty on turn radius was also uniform and as expected (Figure 27). The effect of thrust-to-weight ratio on turn radius was small for initial velocities below the corner velocity and very small for initial velocities above the corner velocity (Figure 28). For the low speed runs the effect of thrust-to-weight ratio was as expected--increase in thrust-to-weight ratio results in a decrease in turn radius. For the high speed runs the effect was not uniform throughout the turn.

This investigation, based on a minimum time turn, cannot consider many aspects of the advantages and disadvantages of thrust vectoring. Several advantages are discussed in two articles by Brown. Discussions with an Air Force pilot who has flown the Harrier in simulated air-to-air combat brought out that there is a very significant capability to bring guns to bear with the thrust-vectored aircraft in situations where the conventional aircraft could not do so. The advantages of in-flight thrust reversing are discussed by McCormick and Koepcke. The work by Humphreys et al should provide insight on the effects of varying thrust during the turn.

CONCLUSIONS AND RECOMMENDATIONS

For initial velocities below the corner velocity, there is a small but consistent advantage for the thrust-vectored aircraft for all thrust-to-weight ratios investigated and for weight penalties up to 25% of the conventional aircraft weight. The differences between the conventional and thrust-vectored aircraft are greatest for initial velocities above the corner velocity and increase with velocity. Although it is difficult to determine which aircraft has the advantage in this velocity range, the results indicate that the thrust-vectored aircraft has the advantage. A more detailed study is definitely justified.

Within the framework of the minimum time turn problem, the effects for turns greater than 180° should be investigated. The effect of limitations on the thrust angle should also be investigated within this framework. Further work should be done in air-to-air combat simulators. The bank angle and thrust angle histories should be helpful to the pilots participating in the simulation and to pilots flying aircraft such as the Harrier.

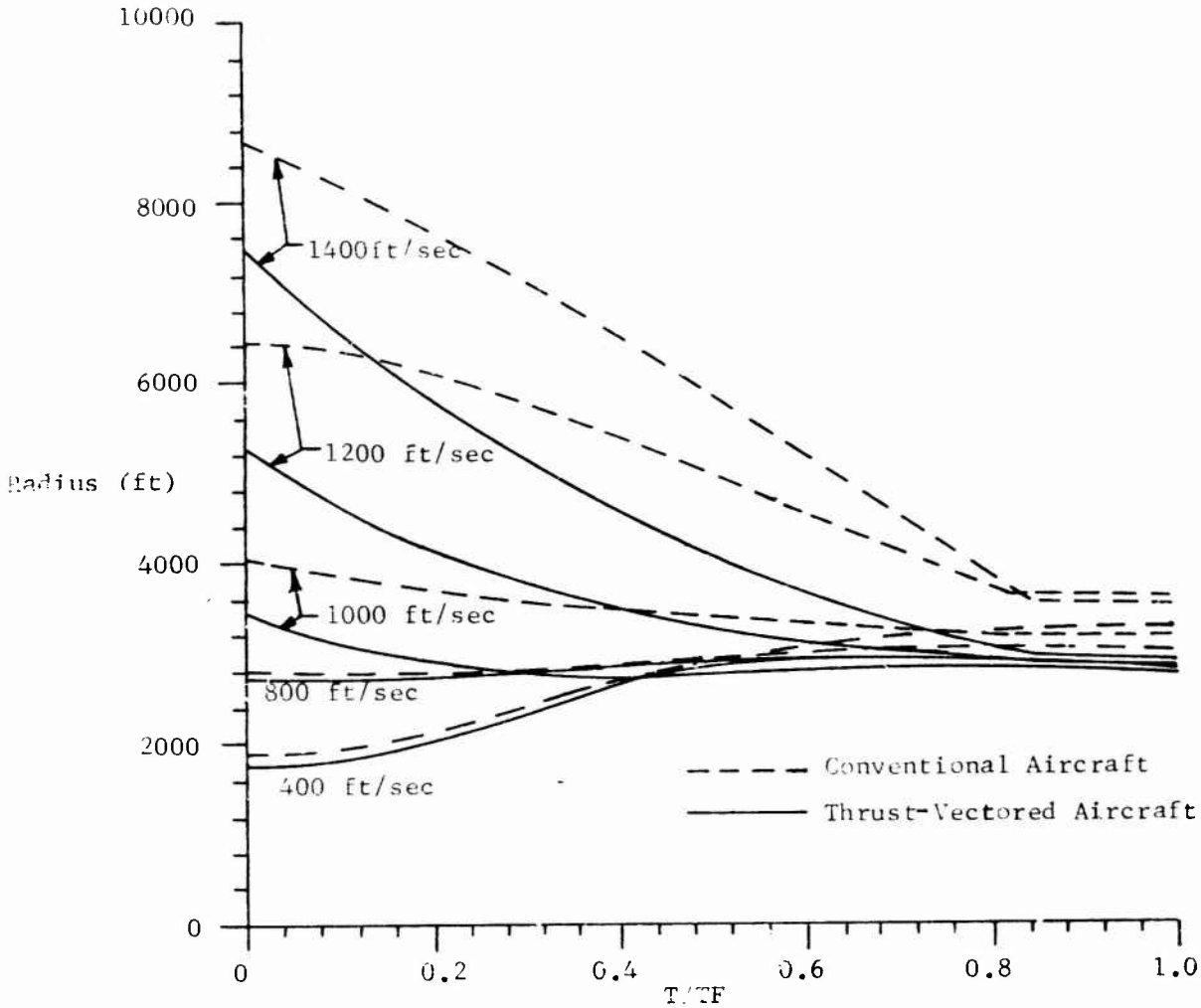

Figure 26. Turn Radius-Effect of Initial Velocity

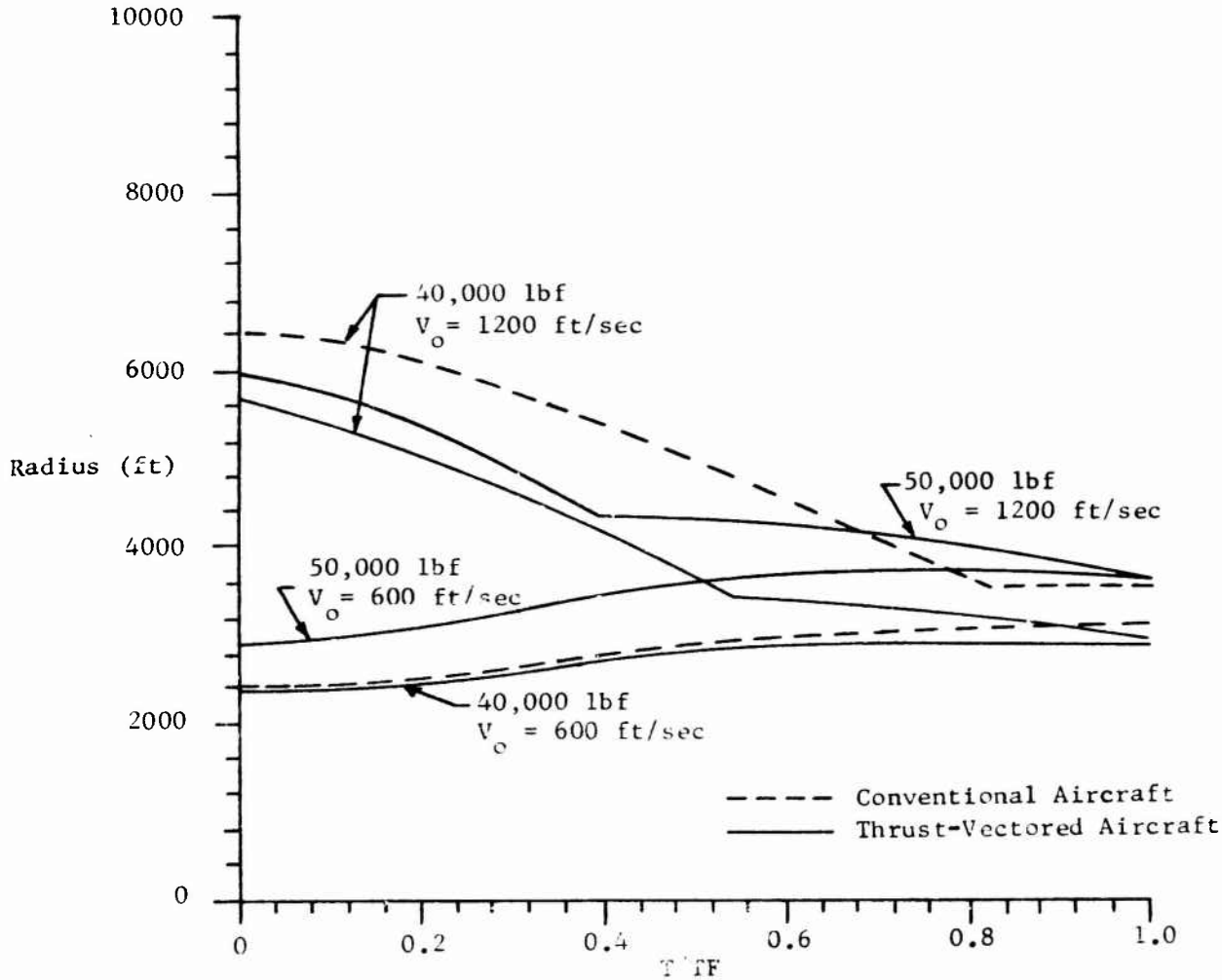

Figure 27. Turn Radius-Effect of Weight Penalty

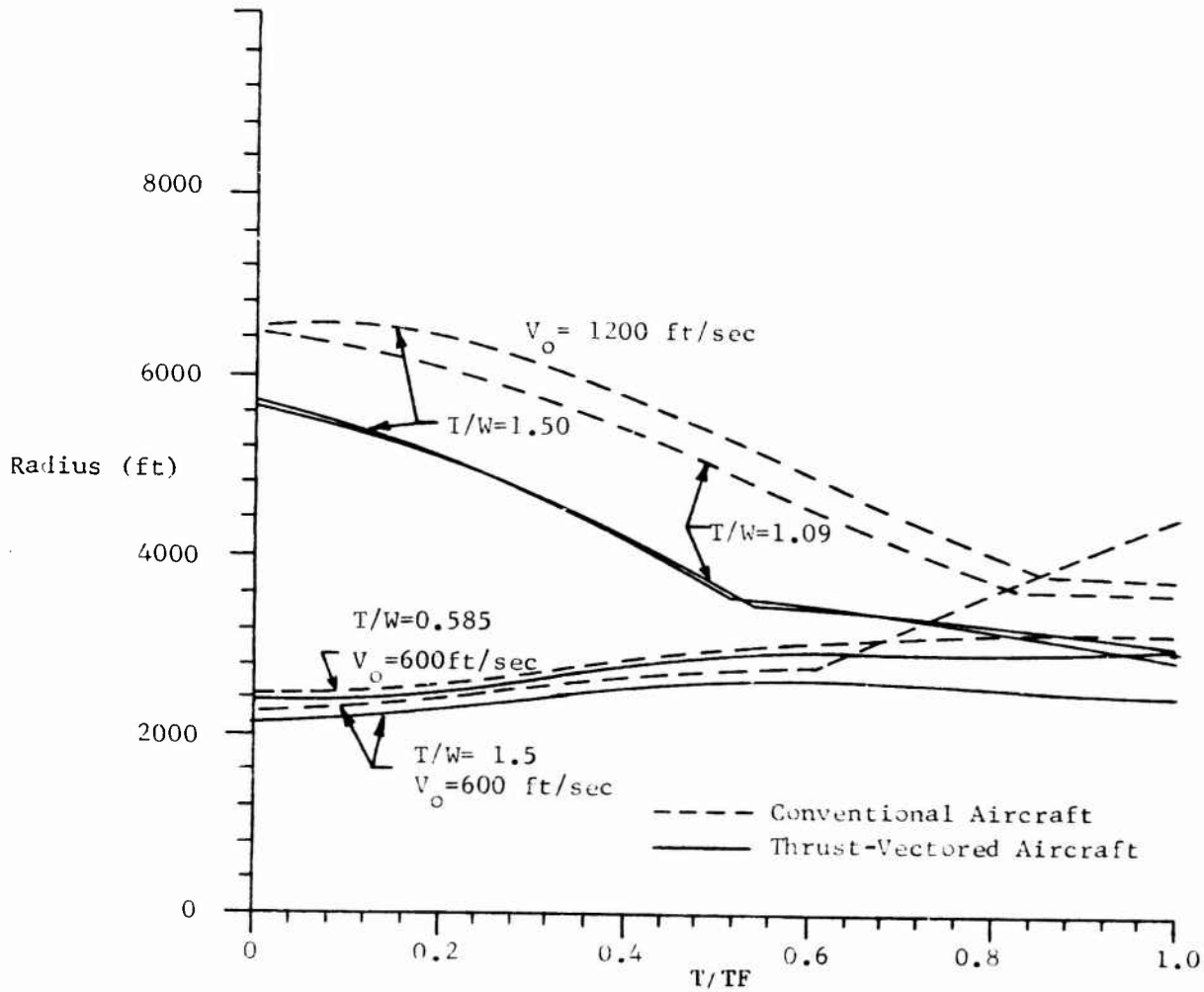

Figure 28. Turn Radius-Effect of Thrust-to-Weight Ratio

LIST OF REFERENCES

1. Brown, David A., "Vectored-Thrust Maneuverability Explored," Aviation Week and Space Technology, December 13, 1971, pp. 36-39.

2. Brown, David A., "Thrust Vectoring to Aid Combat," Aviation Week and Space Technology, January 15, 1973, pp. 46-48.

3. Hines, Jerry D., "A Numerical Technique for Optimal Control Problems with Initial Conditions," Department of Aeronautics Technical Report DFAN TR 73-3, USAFA, June 1973.

4. Hines, Jerry D., and Davis, Duane M., "A Computer Program for Aircraft Optimal Control Problems," Department of Aeronautics Technical Report DFAN TR 73-4, USAFA, July 1973.

5. Humphreys, Robert P., Hennig, George P., Bolding, William A., and Helgeson, Larry A., "Optimal 3-Dimensional Minimum Time Turns for an Aircraft," The Journal of the Astronautical Sciences, Vol XX, No. 2, Sep-Oct 1972, pp. 88-112.

6. McCormick, R.L., and Koepcke, W.W., "Capabilities of In-Flight Thrust Reversing on Tactical Aircraft," Air Force Flight Dynamics Laboratory Report AFFDL-TR-67-120, Wright-Patterson AFB, Ohio, October 1967.

7. Salvadori, M.G., and Baron, M.L., Numerical Methods in Engineering, Prentice-Hall, Inc., Englewood Cliffs, N.J., 1961.